Pinaceae Fir Resins as Natural Dielectrics for Low Voltage Operating, Hysteresis-Free Organic Field Effect Transistors

Jelena Ivić, Andreas Petritz, Cristian Vlad Irimia, Bilge Kahraman, Yasin Kanbur, Mateusz Bednorz, Cigdem Yumusak, Muhammad Awais Aslam, Aleksandar Matković, Klara Saller, Clemens Schwarzinger, Wolfgang Schühly, Annika I. Smeds, Yolanda Salinas, Manuela Schiek, Felix Mayr, Chunlin Xu, Christian Teichert, Mariana Osiac, Niyazi Serdar Sariciftci, Barbara Stadlober, and Mihai Irimia-Vladu*

Natural dielectrics are emerging nowadays as a niche selection of materials for applications targeting biocompatibility and biodegradability for electronics and sensors within the overall effort of scientific community to achieve sustainable development and to build environmental consciousness. The two natural resins analyzed in this study, silver fir and Rocky mountain fir demonstrate robust dielectric properties and excellent film forming capabilities, while being trap free dielectrics in high-performance organic field effect transistors (OFETs) operating at voltages as low as 1 V. Immense research possibilities are demonstrated through the avenue of inorganic nanofillers insertions in the natural resins film, that opens the door for fabrication of very low voltage OFETs with high dielectric constant insulating layers.

1. Introduction

We live engulfed in a world of electronics where is hard to imagine a single day without the assistance of modern technology. The impressive achievements of our time could be explained by the ongoing electronics revolution where inorganic materials with their archetypical examples like silicon (as semiconductor) or silicon dioxide (as dielectric) remain the core elements. Fifty years or more of continuous research and technological adjustments have generated nanoscale-controlled functionalities where active

J. Ivić, A. Petritz, C. V. Irimia, B. Stadlober, M. Irimia-Vladu
Joanneum Research Forschungsgesellschaft
Materials
Franz-Pichler Str. Nr. 30, Weiz 8169, Austria

J. Ivić, M. Osiac
University of Craiova
Department of Physics
Craiova 200585, Romania

C. V. Irimia, B. Kahraman, Y. Kanbur, M. Bednorz, C. Yumusak, M. Schiek,
F. Mayr, N. S. Sariciftci, M. Irimia-Vladu
Johannes Kepler University Linz
Institute of Physical Chemistry
Linz Institute for Organic Solar Cells (LIOS)
Altenberger Str. Nr. 69, Linz 4040, Austria
E-mail: mihai.irimia-vladu@jku.at

Y. Kanbur
Department of Chemistry
Karabük University
Baliklarkayasi Mevkii, Karabük 78050, Turkey

M. A. Aslam, A. Matković, C. Teichert
Institute of Physics
Montanuniversität Leoben
Franz Josef Strasse 18, Leoben 8700, Austria

K. Saller, C. Schwarzinger
Institut for Chemical Technologies of Organic Materials
Johannes Kepler University Linz
Altenberger Str. Nr. 69, Linz 4040, Austria

W. Schühly
Institute of Biology
Karl-Franzens University of Graz
Universitätsplatz 2, Graz 8010, Austria

A. I. Smeds, C. Xu
Laboratory of Natural Materials Technology/Wood and Paper Chemistry
Åbo Akademi University
Porthansgatan 3-5, Åbo/Turku 20500, Finland

Y. Salinas
Institute of Polymer Chemistry
Johannes Kepler University Linz
Altenberger Str. 69, Linz 4040, Austria

M. Schiek
Johannes Kepler University Linz
Center for Surface and Nanoanalytics (ZONA)
Altenberger Str. 69, Linz 4040, Austria

F. Mayr
Institute of Applied Physics
Johannes Kepler University Linz
Altenberger Str. 69, Linz 4040, Austria

M. Irimia-Vladu
Johannes Kepler University Linz
Institute of Physical Chemistry
Linz Institute for Organic Solar Cells (LIOS)
Altenberger Str. Nr. 69, Linz 40040, Austria

materials are produced and deposited in a highly precise, controlled, and organized manner starting at the atomic level, with an impressive level of performance. Nevertheless, the gourmand demand of the market for electronics is also leading to a series of unfortunate and undesirable consequences: i) a massive amount of waste electrical and electronic equipment (WEEE),[1] and ii) a rapid exhaustion of the already scarce natural elements such as gallium and indium. On top of it, there is also an energy imbalance when processing inorganic materials-based electronic devices, with the oxidation process of inorganic dielectrics requiring energies approaching petajoules.[2,3] In our energy and resource-constrained world, both the above-mentioned energy loss and the aggressive resource exploitation become unacceptable.[4,5] Therefore, a paradigm shifts of the way we control both the resource exploitation and the electronics disposal is required, since only a finite portion of electronics is a priory designed and ultimately managed to be collected and recycled.[6]

In their quest to solve the above-mentioned energy deficiency and material availability puzzle, scientists are often inspired both by the apparent simplicity and by the true complexity of nature; dreaming to mimic nature for creating a world of engineered electronic functions, like for example the efforts of reproducing various natural processes.[7,8,9] Nature is nothing but an extremely efficient energy consumption engine that we could rely on for infinite inspiration.[10,11,12] The diversity of natural materials offers a plethora of unexplored phenomena to researchers, and starts already to open new fields in physics and chemistry as well as materials engineering.[13,14,15,16] An exciting area of cross-disciplinary engineering currently emerging is the implementation of natural or nature-inspired, "green" materials for various electronic devices interfaced with living matter.[17,18,19] Here physics, materials science, electrical and mechanical engineering contribute to the success of the emerging field by designing novel biocompatible (active or passive) materials, conceiving device and circuit layouts, selecting the desired packaging strategy, all of them formulated to accomplish the outcome of the integration of bioelectronics with living tissue[20,21,22,23,24] Bio-origin and bio-inspired materials allow in reality for accomplishing far more ambitious goals, like for example fabrication of biodegradable electronics able to safely decompose at the end of their life cycle in order to minimize the costs associated with recycling and the management of environmentally hazardous waste streams.[25,26,27] The last years have witnessed a series of milestone contributions which inspired researchers in building up entirely new research directions by applying natural or nature inspired biodegradable or biocompatible organic materials in situations where highly rigid inorganic materials fail.[24,28]

As our contribution to the fast pace advancing field of natural and bio-origin / bio-derived materials for electronics, we investigated the dielectric properties of two natural resins, silver fir, and Rocky mountain fir. The two *Pinaceae* fir resins were collected from living trees from the area of Graz, Austria (silver fir) and from the Nez Perce National Forest in Northern Idaho, USA (Rocky mountain fir); they were simply solubilized in pure ethanol solution, filtered through a hydrophilic membrane and used to cast dielectric films, without further purification. We demonstrate in this study that the two natural resins stemming from *Pinaceae* trees have robust dielectric properties and excellent film forming capabilities, while being trap-free dielectrics in high-performance organic field effect transistors (OFETs) operating at voltages as low as 1 V.

2. Experimental Description

The resins employed in this work were collected from living trees, and subsequently were solubilized in pure ethanol (99.9%) in 0.1 g ml^{-1} concentration by heating the solution while stirring for 30 min at 50 °C. The solution was filtered through a Chromafil, 0.2 µm pore size hydrophilic filter paper and then diluted to the concentration employed for depositing thin films in this work, i.e., 25 mg ml^{-1}, 20 mg ml^{-1}, 10 mg ml^{-1}, and 2.5 mg ml^{-1} respectively. In the case of silver fir, we also ran an experiment with a stock solution (2 mg/ml concentration) containing insertions of titania (TiO$_2$, a commercially available product from Merck, product code 718 467, with declared particle size of 21 nm). We dispersed titania (5 mg ml^{-1}) in a solution concentration of 2 mg ml^{-1} resin in ethanol in the respective case. All the resin thin films investigated in this work were spin-coated with a rotation speed of at least 2500 rpm and then dried on the top of a hot plate in air for 1 hour at a temperature not exceeding 80 °C.

We performed gas chromatography measurement for the two resins in this study by dissolving them in 2 ml ethanol and used as solutions containing ≈200 mg per sample. Of each solution, 100 µl was withdrawn and transferred to a tarred (with a microbalance) in a 1.5 ml glass vial. The solvent was evaporated to dryness using a stream of nitrogen, and then the vials were kept in a vacuum oven (at 40 °C) for ≈30 min. After cooling to room temperature, the vials were weighed for determination of the dry extract weight. A volume of 1.0 or 1.5 ml of acetone was added, and the vials were kept for circa 1 min in an ultrasonic bath. A volume corresponding to ≈0.6 mg of each dry resin was withdrawn and transferred to a 6 ml test tube. 2 ml of a solution containing 40 µg each of four internal standards (ISs) was added, and the solvent was evaporated to dryness using a stream of nitrogen in a 40 °C water bath. Silylation reagents were added: pyridine-BSTFA-TMCS 20:80:20 µl, and the tubes were kept in an oven at 70 °C for 30 min. After this, the solutions were transferred using Pasteur pipettes to 1.5 ml GC vials with a glass insert. Circa 1 µl of each sample was injected to the GC-MS. Identifications was done by comparing the mass spectra with those in spectra databases: NIST12/Wiley 11th and our own database (i.e., ABÖ Akademi, Finland). The peak areas were integrated and the concentration of each compound was calculated by dividing the peak area with that of the IS (heneicosanoic acid for all compounds eluting before cholestadiene, and cholesterol or betulinol for cholestadiene and lignans). Then, the result was multiplied by the added amount of IS, and the results was divided by the amount of dry resin taken for the analysis.

In addition, we performed at the Institute for Chemical Technologies of Organic Materials, Johannes Kepler University Linz, Austria gas chromatography and HPLC high-resolution MS analyses of all samples and also pyrolysis-GC-MS analysis as this technique does not discriminate insoluble fractions

**ADVANCED
SCIENCE NEWS**

www.advancedsciencenews.com

**ADVANCED
SUSTAINABLE
SYSTEMS**

www.advsustainsys.com

of the resins. The molar mass distribution of the resins was obtained by size exclusion chromatography. For HPLC-MS: roughly 10 mg of sample were mixed with 1 mL of acetonitrile and sonicated for 5 min, centrifuged and the soluble fraction analyzed. The characterization of resin compounds was performed using a Thermo Scientific Surveyor HPLC system coupled to a LTQ Orbitrap Velos mass spectrometer. Compounds were separated on a Thermo Scientific Accucore C18 column (150 mm × 3.0 mm, 2.6 um particle size) using a gradient with mobile phase A containing 0.1% formic acid in water and mobile phase B containing 0.1% formic acid in acetonitrile, at a flow rate of 0.5 mL min^{-1}. The elution gradient starting conditions were 95% A and 5% B. After 2 min of equilibration time, the proportion of B was increased to 20% at 8 min, to 40% at 12 min, to 60% at 15 min, and to 95% at 19 min and held constant for another 4 min. UV detection was done by a photodiode array detector and mass spectra were recorded with an atmospheric pressure chemical ionization interface in FT mode with a resolution of 30 000. For pyrolysis-GC-MS: in order to achieve better performance in the analysis of natural products pyrolysis in the presence of tetramethylammonium hydroxide (also known as thermally assisted hydrolysis and methylation) has been performed.[29] Experiments were carried out with a CDS Pyroprobe 5250 pyrolyzer (CDS Analytical Inc.) coupled to a Trace GC Ultra (Thermo Electron Corp.) equipped with a capillary column Restek RTX35 (30 m × 0.32 mm × 0.25 μm), and a quadrupole mass spectrometer MD 800 (Fisons Instruments). 5 μL of saturated aqueous tetramethylammonium hydroxide (TMAH, Fluka) solution were added to ≈100 μg of sample and pyrolysis was performed at 550 °C for 10 s. The pyrolyzer interface was set at 300 °C and the injector at 280 °C. The GC column temperature conditions were as follows: initial temperature 50 °C, hold for 2 min, increase at 20 °C min^{-1} to 300 °C, and hold this temperature for 10 min. Helium gas flow was set to 0.8 mL min^{-1}, the split flow was 14 mL min^{-1}. Mass spectra were recorded under electron impact ionization at 70 eV electron energy in the range from m/z 15–400. Identification of the compounds was done by comparison of the mass spectra with NIST 2011 electronic library and literature.[30] For size exclusion chromatography: the samples were mixed with tetrahydrofurane (THF) and the insoluble part filtered off.

Attenuated total reflection Fourier-transform infrared (ATR-FTIR) spectra were measured on a Bruker Vertex 80 FTIR spectrometer equipped with a Bruker Platinum ATR unit and a liquid N$_2$-cooled mercury cadmium telluride (MCT) detector at the Department of Physical Chemistry, Linz Institute for Organic Solar Cells of Johannes Kepler University Linz, Austria. Spectra were recorded with a resolution of 1 cm^{-1} and averaging of 200 scans. Solid resin material for ATR-FTIR measurements was obtained from ethanolic solutions of the resins by depositing the resin on glass substrates via drop-casting, drying the resulting film at 75 °C and carefully scraping off resin material from the substrate.

AFM and KPFM (amplitude modulated-AM) measurements of bare resin films on gold-coated glass substrates were performed using Horiba/AIST-NT Omegascope AFM system at the Institute of Physics, Montanuniversität Leoben, Austria. Nu-nano SPARK probes were used (spring constant ≈42 N m^{-1}, resonant frequency ≈350 kHz, tip radius below 30 nm). For AFM/KPFM experiments, the gold back electrode of the resin films was grounded. AM-KPFM measurements providing contact potential differences (CPD)[31] were carried out in a two-pass mode, with the probe lifted by 25 nm in the second pass. Root mean square (RMS) data is proved for both the topography roughness and the CPD fluctuations as an average with a standard deviation considering five arbitrarily chosen 10 × 10 μm^2 areas of each resin sample. Topography and CPD images were processed in the open-source software Gwyddion v2.56. For topography images zero-order line filtering was applied and leveling of the base plane. For CPD images only zero-order line filtering was applied.

Thermogravimetric analyses were carried out with a TGA/PerkinElmer Q5000, using platinum pans and measurements from 70 to 900 °C, with heating rate of 10 °C min^{-1} under nitrogen (25 mL min^{-1}) at the Institute of Polymer Chemistry, Johannes Kepler University Linz, Austria. For the TGA investigation, the two fir resin samples (in an amount ranging from 5 to 15 mg) were analyzed employing an identical experimental heating setup and procedure.

For determining the complex refractive index at optical frequencies, resin layers have been prepared by spin coating and subsequent drying at 60 °C on fused silica substrates, with the experiment carried at the Center for Surface and Nanoanalytics of Johannes Kepler University Linz, Austria. Standard ellipsometry scans in reflection and transmission intensity data have been recorded with a J.A. Woollam M 2000 DI ellipsometer covering a spectral range from 195 to 1685 nm. The transmission measurements were limited by the fused silica substrate which was sufficiently transparent down to 230 nm. Data were analyzed with Complete EASE starting with a Cauchy layer in the transparent range to fit the layer thickness. Conversion to a transparent B-spline (Kramers-Kronig consistent mode on, 0.2 eV spectral resolution) with automated wavelength expansion fit gave the complex refractive index of the resin layers. Ellipsometric and transmission data were analyzed jointly, and backside reflection have been included in the fitting.

All the dielectric related investigations, i.e., the dielectric constant, dielectric strength (breakdown field), and impedance spectroscopy in the frequency range spanning 1 MHz to 1 mHz for all the resins were accomplished with the two resins sandwiched in metal-insulator-metal configuration at the Department of Physical Chemistry, Linz Institute for organic solar cells of Johannes Kepler University Linz, Austria. The instrument employed in the dielectric measurements was a Novocontrol Broadband Dielectric/Impedance Spectrometer (Novocontrol Technologies GmbH) equipped with a 500 V DC booster. Each resin was spin-coated on top of a 80 nm thick, 1 mm wide plain aluminum electrode, dried for 1 hour in ambient air at 80 °C, and the respective device terminated by the deposition of another layer of 80 nm thick, 1 mm width aluminum electrode in a cross configuration to the bottom electrode. For the dielectric strength measurement, the MIM device was clamped between two alligator clips and connected to a Novocontrol impedance analyzer with a DC booster instrument working to 500 V DC voltage. A DC voltage scan was passed to the MIM device, starting from 0 V, with an incremental step of 2 V and 2.5 sec wait time at each particular applied voltage. The breakdown voltage was taken as the one for which a sudden loss
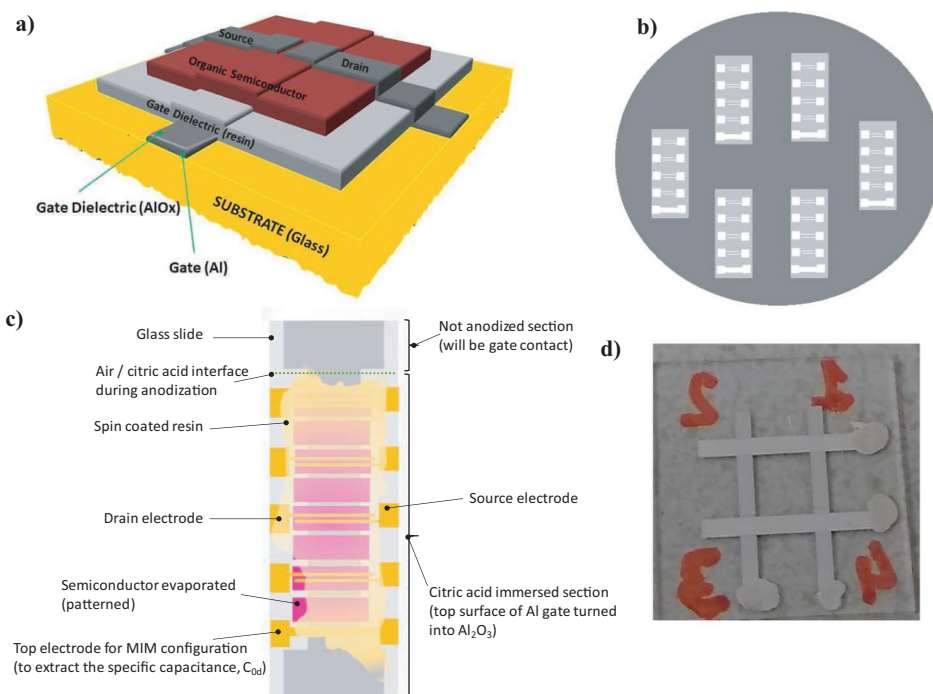
Figure 1. Design structures utilized in this work for OFET and dielectric measurements: a) Schematic of the staggered bottom gate-top contact OFET architecture; b) Photograph of the source-drain shadow mask utilized for the top contact deposition via physical vapor deposition. The mask features 4 contacts for S-D deposition and one contact as a continuous top electrode utilized for the capacitance measurement; c) Schematic of the final display of the fabricated OFET that is ready to be measured in the probe station. The semiconductor is patterned through 8 shadow holes as presented in the schematic of this figure. Our fabrication design allows us to employ two shadow masks for two successive S-D depositions to generate alternative S-D contacts in case different electrodes are needed (n-type or p-type injecting electrodes). For the particular development of this work, we deposited all the eight patterned electordes with the same type of metal, i.e., gold for pentacene in each case in two successive evaporations; d) photograph of the metal-insulator-metal (MIM) structure employed for all the dielectric measurements (impedance data, dielectric constant, breakdown field) consisting of spin-coated resin film sandwiched between two bottom and two top electrodes, each of 1 mm in width. The four contact pads were decorated with silver paste to increase the robustness of the deposited aluminum electrode during clamping in the Novocontrol impedance measurement instrument. Given the proximity of the 4 MIM sandwich electrodes, the reproducibility of the results was very high on each fabricated substrate, as the one shown above. The resin film was fully transparrent, highly homogeneous, and hardly visible by naked eye.

of several orders of magnitude of the dielectric capacitance was observed on the measurement display. In the case of the analyzed resins, the breakdown voltage was nonambiguously determined, since the resins did not break gradually, but rather sharp, as will be shown in a graph in the text of this report. The breakdown field was calculated by dividing the breakdown voltage to the measured thickness of the film via profilometry. We analyzed four glass slides (in total 16 MIM samples, see **Figure 1**d)) for each of the two resins for both dielectric and breakdown field measurements and observed a very nice reproducibility among the samples of each particular resin.

OFET fabrication and all the OFET related measurements and investigations were performed at Joanneum Research Materials in Weiz, Austria. The gate electrode of the fabricated OFETs comprised either a bilayer of aluminum oxide and resin thin film as capping layer, or simply the resin as stand alone gate dielectric. The aluminum oxide was grown electrochemically using a previously reported recipe[32] that was optimized over the years in our laboratories (Joanneum Research Materials and JKU Linz).[33,34] The setup employed in the anodization process involved a current-voltage source meter, Keithley 4ZA4 with the positive terminal connected to the active electrode (i.e., the aluminum gate layer to be anodized) and
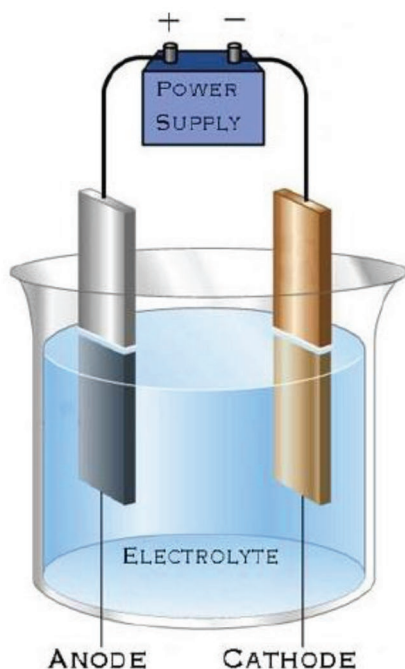
the negative terminal to the platinum reference electrode, see **Figure 2**). The citric acid solution concentration is very critical for the quality of the electrochemically grown dielectric layer. We used a solution of identical concentration as previously reported by Mardare et al.,[35] i.e., 0.265 g citric acid and 2.57 g sodium citrate in 100 ml deionized water producing a pH of ≈6.0. A pH of the anodization solution close to neutral is critical in obtaining a smooth and densely anodized layer of aluminum oxide. During anodization, considering Al^{3+} and oxygen-containing anions (O^{2-} or OH^-) mobile under the applied electric field (E), the reactions that occur at both the interfaces of aluminum to aluminum oxide and aluminum oxide to electrolyte are:

At the aluminum/aluminum oxide interface:

$$Al \rightarrow Al^{3+} + 3e^- \tag{1}$$

$$2Al^{3+} + 3O^{2-} \rightarrow Al_2O_3 \tag{2}$$

At the aluminum oxide/electrolyte interface:

$$2Al^{3+} + 3O^{2-} \rightarrow Al_2O_3 \tag{3}$$

Figure 2. Schematic of the anodization setup. The anode is the gate electrode to be anodized, the cathode is platinum reference electrode, and the electrolyte is citric acid containing citrate buffer in 18.2 MΩ deionized water.

$$Al_2O_3 + 6H^+ \rightarrow 2Al^{3+} + 3H_2O \tag{4}$$

$$Al^{3+}(ox) \rightarrow Al^{3+}(aq) \tag{5}$$

The thickness of the aluminum gate electrodes that were subsequently anodized was 80 nm for all the OFET devices, and the anodization was carried out in a clean room environment (at Joanneum Research Materials mbH, cleanroom class 6 for nano-structuring, novel electronic components, and sensors – certified according to ISO 14 644). Importantly, the aluminum used for evaporation to obtain the gate electrode had a purity of 99.999% (ChemPUR GmbH) and the respective gate electrode layer was evaporated at a fast rate of ≈4–5 nm sec^{-1}, which proved beneficial for generating a very smooth metal layer, and allowed subsequently obtaining a very high-quality aluminum oxide via anodization process. The anodization voltage of this study was set to 10 V (for most of the devices employed here), while maintaining in this process a steady current of 15 mA. After reaching the 10 V compliance, the sample was allowed to slowly continue to anodize (annihilate any possible defects or un-anodized pockets in the layer of generated Al$_2$O$_3$ material) until the final current decreased to ≈4.5 µA. A typical thickness of the anodized layer is given by the equation[35]:
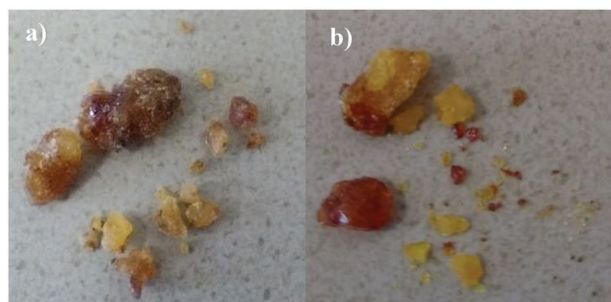
$$d = \alpha(V - V_{ox}) \tag{6}$$

where α is the oxide forming factor, with a value of 1.6 for aluminum; V is the applied maximum voltage of anodization (i.e., typically 10 V in our case for most of the devices) and V_{ox} is the voltage necessary to generate the native oxide (i.e., the layer

that forms naturally when aluminum is exposed to ambient air), and has a value of ≈−1.35 V for aluminum.[36] The measured bi-layer capacitance using a Novocontrol impedance analyzer instrument matched well the calculated capacitance of the aluminum oxide layer of ≈18 nm Al$_2$O$_3$. The semiconductor material, pentacene in this study, was purchased by Aldrich, purified two times by sublimation, and deposited in a physical vapor deposition (PVD) system (Univex), using identical recipes of deposition (vacuum level, temperature ramp, the deposition rate of 0.2–0.3 Å sec^{-1}, etc.) for both resins. We employed an identical transistor geometry for all the OFETs fabricated in this study, with a 2 mm wide gate electrode and channel dimensions of 35 µm in length (L) and 2 mm width (W). In this study we did not attempt to optimize the semiconductor deposition in order to obtain record hole or electron mobilities[37,38] and fabricated 3 batches of 48 OFETs on each batch (i.e., 1 batch contained 6 glass slides, 8 OFETs per slide, see Figure 1b) for each resin employed in the study. All the fabricated OFETs were measured with a probe station situated in a glove box under nitrogen atmosphere, in Joanneum Research Materials laboratory. The architecture of the OFET device employed all throughout this work involved a staggered bottom gate-top contact design, as schematically presented in Figure 1a,c. In Figure 1b is presented the picture of the source and drain shadow mask employed for the topcontact deposition (i.e., source S, and drain, D). The respective mask allows deposition of one top continuous electrode per glass slide in a section of the gate electrode where the semiconductor has not been patterned (see bottom section of Figure 1c) where a fully fabricated OFET slide is presented schematically). The respective electrode constitutes the MIM geometry used for extracting the specific capacitance of the respective slide. Our fabrication design allows patterning 8 patches of semiconductor and the possibility to develop 4 pairs of source and drain electrodes by physical vapor deposition in one evaporation step (Figure 1b,c). In a subsequent evaporation, one has the option to deposit with another S-D mask another set of 4 electrodes (on the semiconductor patches that were masked during the first S-D deposition), either of the same metal or of a different one. In our work involving Pinaceae fir resins, we deposited in the second step the same metal (Au for pentacene), since our work in this publication was aimed at investigating the dielectric and not at examining a novel organic semiconductor for which a suitable metal with appropriate work function for charge injection was necessary to identify.

3. Results and Discussion

3.1. Resins Composition Analysis

The two collected resins have a similar appearance, as it is demonstrated by the recorded photographs presented in **Figure 3**. The wood and bark of silver fir (*abies alba*) is composed of several polyphenols[39] with antioxidative properties in animals and human subjects[40] and are currently employed in various treatments aimed at atherosclerosis prevention, cardioprotective effects, reduction of glycemic response after meal, etc. Tavčar Benković et al.[41] as well as Vasincu et al.[39]

**ADVANCED
SCIENCE NEWS**

www.advancedsciencenews.com

**ADVANCED
SUSTAINABLE
SYSTEMS**

www.advsustainsys.com

Figure 3. Photograph of the collected resins: a) silver fir and b) Rocky mountain fir.

identified in the bark of *abies alba* six types of phenolic acids (gallic, homovanillic, protocatehuic, p-hydroxybenzoic, vanillic, and p-coumaric), three types of flavonoids (catechin, epicatechin and catechin tetramethyl ether) and eight types of lignans derivatives (taxiresinol, 7-(2-methyl-3,4-dihydroxytetrahydropyran-5-yloxy)-taxiresinol, secoisolariciresinol, laricinresinol, hydroxymatairesinol, isolariciresinol, matairesinol and pinoresinol). Gas chromatography analysis of the resin investigated in this work showed that the chemical content and composition of silver fir was rich in resin acids, and among them, dehydroabietic acid was dominating (12%), followed by palustric (4.6%) and isopimaric acid (3.2%). Other notable detected resin acids were neoabietic, abietic, and pimaric acid at concentrations of 0.25%, 0.24%, and 0.78%, respectively. Thunbergol and pinoresinol lignans were also present in significant levels (i.e., 1.5% and 1.9%, respectively). Other detected diterpenoids were, e.g., isopimarol and isopimaral (0.14% and 0.049%, respectively). Cholestadiene accounted for 0.054% of the resin weight. The diterpenoids accounted altogether for 31% of the resin weight (GC eluting compounds altogether 38%).

The resin of Rocky mountain fir (*abies lasiocarpa*) appears in fresh wounds of the bark of the tree, and similarly to silver fir is yellow-brown in color appearance, as Figure 3 shows.[42] Not surprisingly, the chemical content and composition of rocky mountain fir resin was comparable to that of silver fir, although the resin acid composition was slightly different. Dehydroabietic acid dominated among the resin acids (10.0%), followed by abietic (3.58%), isopimaric (3.00%), palustric (2.73%), pimaric (1.92%), pimaradienoic (2.24%), and neoabietic acid (1.50%). Other notable diterpenoids were oxidised resin acids (altogether 4.03%), pimarol (1.20%), isopimarol (0.53%), pimaral, and isopimaral (0.28% and 0.21%, respectively). Cholestadiene accounted for 0.086% of the resin weight. The content of unidentified GC eluting compounds was also higher (8.4% compared to 3.7% in the case of silver fir). The results of GC-MS analysis are presented in **Table 1**. **Tables 2** and **3** present the full list of identified compounds by high-performance liquid chromatography (HPLC) and size exclusion chromatography (SEC) methods respectively. The chemical structure of the most prominent constituents of the two fir resins is presented in **Figure 4** below.

Figure 5a presents the ATR-FTIR spectrum of silver fir resin that displays a pronounced broad carboxylic acid O−H stretching band at 3600 − 2500 cm^{-1} as well as carboxylic acid

Table 1. Gas chromatography analysis displaying the concentrations (mg/g dry ethanol extract) in species of coniferous resins was analyzed in this work. Legend: RA = resin acid; nd = not detected.

Component	Silver fir	R.M. fir
Mono- and sesquiterpenoids		
β-Phellandrene	nd	1.13
Cadinenes (β, δ)	0.254	nd
11-Hydroxy-eremophil-1(10)-ene	1.21	nd
Sum	1.46	1.13
Diterpenoids		
RAs:		
Secodehydroabietic acids	1.96	nd
Pimaric acid	7.76	19.2
Sandaracopimaric acid	nd	4.24
Isopimaric acid	32.0	30.0
Abietatetraenoic acid(s)	1.43	1.93
Palustric acid	46.4	27.3
Dehydroabietic acid (DeAb)	119	100
Methyl dehydroabietate	0.496	nd
Abietic acid (Ab)	24.1	35.8
Neoabietic acid	25.2	15.0
8,15-Pimaradien-18-oic acid	nd	22.4
Sum	258	256
Oxidised RAs:		
Hydroxy-DeAbs	13.9	19.4
Hydroxy-Ab(s)	7.88	13.2
Hydroxy-RA	0.830	1.31
Dihydroxy-DeAb(s)	1.51	4.59
Hydroxy-7-oxo-DeAb	0.799	1.76
Sum	24.9	40.3
Other diterpenoids:		
Thunbergene(s)	4.94	nd
Thunbergol	15.5	nd
Cis-abienol	1.92	nd
Pimaral	nd	2.80
Isopimaral	0.492	2.07
Palustral	1.44	nd
Dehydroabietal	0.971	nd
Pimarol	nd	12.0
Isopimarol	1.39	5.35
Palustrol	1.45	nd
Dehydroabietol	1.70	0.735
Neoabietol	0.738	nd
Sum	30.5	22.9
Small-molecular aliphatic acids		
Lactic acid	1.19	2.12
Glycolic acid	nd	0.839
3-Hydroxypropanoic acid	nd	0.362
Succinic acid	0.245	0.218
Sum	1.43	3.54

**ADVANCED
SCIENCE NEWS**

www.advancedsciencenews.com

**ADVANCED
SUSTAINABLE
SYSTEMS**

www.advsustainsys.com

Table 1. Continued.

Component	Silver fir	R.M. fir
Fatty acids and alcohols		
n-Hexadecanoic acid	0.744	0.469
n-Heptadecanoic acid	0.872	0.442
n-Octadecanoic acid	nd	nd
n-Hexadecanol	0.269	0.195
Sum	1.88	1.11
Aromatic compounds		
Cinnamic acids	0.355	nd
p-Coumaric acid	0.340	nd
3-Hydroxy-4-methoxybenzaldehyde	0.249	nd
4-Hydroxycinnamic acid	5.43	nd
Lariciresinol	1.63	nd
Pinoresinol	18.8	nd
Sum	26.8	0
Miscellaneous		
Carbonic acid	0.825	nd
Glycerol	0.405	0.701
Cholestadiene	0.538	0.865
Diacetone alcohol	0.421	0.630
Sum	2.19	2.19
IDENTIFIED, SUM	347	327
UNIDENTIFIED PEAKS	37	84
% GC ELUTING	38.4	41.1

overtone vibration bands at 2667 cm^{-1} and 2536 cm^{-1}. The very strong band at 1692 cm^{-1} corresponds to the carboxylic acid C=O stretching vibration, which is characteristic of diterpenoid resin acids.[43,44,45] This corroborates the presence of resin acid compounds as the clearly predominant constituents of the resin as identified by GC-MS. Further indication of the general compositional similarities of silver fir and Rocky mountain fir resin are the largely similar positions of the O−H bending, C−O stretching, and in-plane C−H bending bands in the wavenumber region of 1268 – 1035 cm,[1] and the out-of-plane C−H bending vibrations in the region of 906 – 652 cm^{-1}, respectively. Almost identical positions can be observed for the C−H stretching vibration bands at 3079 – 2868 cm^{-1} and the −CH$_3$ and −CH$_2$− bending vibrations at 1458, 1384, and 1364 cm^{-1}. In comparison to Rocky Mountain fir though, the aromatic C=C stretching vibration bands at 1604 cm^{-1} and 1515 cm^{-1} appear with a higher relative intensity in the case of silver fir resin. This conforms well to the fraction of phenolic lignans such as pinoresinol in the silver fir resin as found by GC-MS analysis of the material, that is absent for Rocky mountain fir. The ATR-FTIR spectrum measured for the investigated Rocky mountain fir resin is shown in b). Similar to silver fir resin, the FTIR spectrum of Rocky Mountain fir clearly shows the predominance of resin acids in the composition of the resin as indicated by the pronounced carboxylic acid features. In a similar fashion

to the bands assignment of silver fir resin, also in the case of Rocky mountain fir, the very broad band at ≈3600 – 2500 cm^{-1} corresponds to the carboxylic acid O−H stretching vibration while the bands at 2656 cm^{-1} and 2533 cm^{-1} can be assigned to carboxylic acid overtone vibrations. The very strong band at 1692 cm^{-1} corresponds to the carbonyl stretching vibration of the −COOH group and is located at a spectral position typically found for resin acids[43,44,45] which was also observed in the above-mentioned resins with predominantly resin acid constituents investigated in this study. The weak band at 3077 cm^{-1} corresponds to the C−H stretching vibration in unsaturated hydrocarbons while the strong bands at 2927–2868 cm^{-1} can be assigned to the C−H stretching in saturated hydrocarbons. The distinct bands in the region of 1458 – 1365 cm^{-1} stem from the bending vibration in methyl and methylene groups. The positions of these bands are largely identical to those found for silver fir resin. The bands in the wavenumber region of 1274 – 1036 cm^{-1} can be assigned to O−H and C−O vibrations of oxygen-containing functional groups and in-plane C−H bending in unsaturated cyclic hydrocarbons. The distinct bands in the low wavenumber region at 905, 882, 822, 707, and 653 cm^{-1} can be attributed to out-of-plane C−H bending in unsaturated hydrocarbons and can be assigned to the different unsaturated aliphatic (e.g., abietic acid, isopimaric acid) and aromatic (dehydroabietic acid) resin acid compounds. The positions and relative intensities of these bands are similar to those measured for silver fir resin which is indicative for largely similar fractions of the main resin acid constituents in both resins as found by GC-MS measurements.

3.2. Surface Investigation

We performed a surface investigation of silver fir and Rocky mountain fir resins via contact angle measurement, atomic force microscopy (AFM), and kelvin probe force microscopy (KPFM), presented in **Figure 6**.

Between the two resins that were deposited in thin-films by spin coating on gold-covered glass, silver fir samples were found to have smaller topography roughness (0.34 ± 0.13) nm, but a bit larger spatial variation of the contact potential difference (CPD) of 4.21 ± 0.55 mV, compared to the respective values of 1.3 ± 0.13 nm and 1.81 ± 0.01 mV for Rocky mountain fir. It is worth mentioning that the RMS roughness of silver fir thin-film rivals the one of plain glass, and both resins in fact have unparalleled film forming characteristics that recommends them for further investigation in electronic devices. While the observed domains in CPD do correspond to topography features, they cannot be attributed merely to the thickness variation. CPD variations observed in the two fir samples are still several times smaller in comparison to silicon dioxide, SiO$_2$ or aluminum oxide, Al$_2$O$_3$ surfaces, where CPD values of 18,2 mV and 82.3 mV respectively were measured in our laboratories. These high potential fluctuations of plain Al$_2$O$_3$ samples could lead to the formation of the interfacial dipoles, resulting in filling and emptying the trap states in the dielectric at the interface to the semiconductor and consequently a pronounced hysteresis between forward and reverse scans in the electrical

**ADVANCED
SCIENCE NEWS**
www.advancedsciencenews.com

**ADVANCED
SUSTAINABLE
SYSTEMS**
www.advsustainsys.com

Table 2. HPLC-HRMS analysis of the soluble fraction of the fir resins.

t_R(UV) / min	MH$^+$	Name	Sum formula		Rocky mountain fir	Silver fir
					% area (UV)	
8.17	165.0544	Hydroxycinnamic acid	$C_9H_8O_3$			15.87
11.47	375.1438	Hydroxymatairesinol	$C_{20}H_{22}O_7$			0.47
11.92	219.1014		$C_{13}H_{14}O_3$			1.82
13.1	341.1382		$C_{20}H_{20}O_5$			13.9
14.83	317.2109		$C_{20}H_{28}O_3$		1.4	
15.01	331.1901		$C_{20}H_{26}O_4$		1.66	
15.39	507.2011		$C_{29}H_{30}O_8$			11.66
15.61	333.2057		$C_{20}H_{28}O_4$		1.16	
16.54	299.2004		$C_{20}H_{26}O_2$		0.82	1.91
17.18	319.2265		$C_{20}H_{30}O_3$		2.06	2.38
17.75	301.2159	Retinoic acid	$C_{20}H_{28}O_2$		2.04	
17.94	299.2003		$C_{20}H_{26}O_2$		0.69	
18.18	315.1952		$C_{20}H_{26}O_3$		2.82	1.44
19.74	301.2159	Dehydroabietic acid	$C_{20}H_{28}O_2$		2.74	2.05
20.26	301.2158		$C_{20}H_{28}O_2$		1.11	
20.62	no mass signal	Overlapping with isopimaric acid			20.04	
20.69	303.2314	Isopimaric acid	$C_{20}H_{30}O_2$		56.12	38.06
21.44	273.2573		$C_{20}H_{32}$			0.23
22.23	287.2367	Retinol	$C_{20}H_{30}O$			0.32
		Total:			92.66	90.11

transfer curves of the OFETs. As a general observation, the slight discrepancies observed between the topography and CPD RMS roughness of the two fir resins are minor. In both cases, their CPD and RMS values are well below commonly used dielectrics as Al_2O_3 or SiO_2 (as exemplified above). Less smooth topography of the Rocky mountain fir resin film could be due to not perfectly optimized thin film deposition. However, the point is that neither of the two films tends to form agglomerates, to de-wet the substrate, or to form different phases (which otherwise would be visible in the CPD maps). We consider that a possible reason for electrostatically more uniform surface of the two fir resins films investigated here is their less hydrophilic behavior than SiO_2, which is indeed confirmed by the contact angle measurements displayed in **Figure 7**.

The contact angle measurement of silver fir solution revealed a hydrophilic surface with a contact angle of ≈68° for water droplet (see Figure 7), with a total surface energy of 50.8 mN m^{-1}. The silver fir and titania insertions (this mixture will be detailed in the following), offered an even more hydrophilic surface with a contact angle with water droplet of ≈40.1°. The surface of Rocky mountain fir resin reveals a hydrophilic layer of ≈72.7° for water droplet. The calculated total energy of the resin was ≈47 mN m^{-1} (Figure 7).

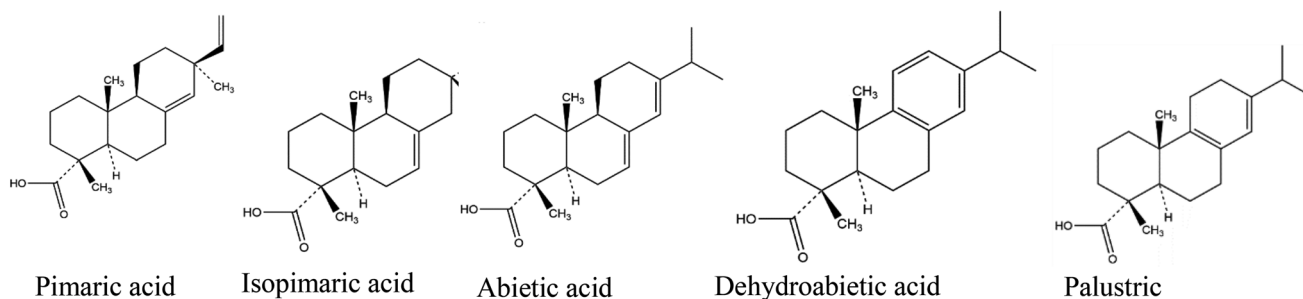**Table 3.** Size exclusion chromatography of the fir resins.

	M_n/g mol^{-1}	M_w/g mol^{-1}	Đ
Rocky mountain fir	308	665	2.2
Silver fir	315	537	1.7

3.3. Thermogravimetric Analysis

Two different pellets of silver fir resin material were evaluated for TGA, stemming from the deposit produced by the same tree. The first pellet was collected in September in 2017 and preserved in a vial in a laboratory cabinet. The second pellet was collected from the respective tree in October 2021. The TGA experiment was carried in October 2021 for both resin samples of silver fir. Not surprisingly, similar decomposition temperatures, and curve transitions were observed (as seen in the corresponding TGAs, **Figure 8**). Here, the first weight loss which occurs below 120 °C because of the evaporation of the adsorbed water, was similarly detected in both resins (0.86% and 0.89% respectively). The second pronounced weight loss was observed between 120°C and 450 °C (≈93 and ≈95% respectively) both centered at 260—261 °C. At higher temperatures, between 450 and 650 °C, a third weight loss had to be accounted for, at ≈541—543 °C (≈7% in both cases). Finally, in both samples, a similar fourth weight loss of ≈0.2% for silver fir 2017 and ≈0.4% for silver fir 2021, was observed in a temperature range spanning from 620 °C to 900 °C, leaving a residual weight of less than 1%.

Considering the similarities in composition and FTIR signal of the two fir resins investigated here, it does not come to a surprise that the Rocky mountain fir resin behavior was in full agreement with the one of silver fir with respect to material decomposition by TGA analysis (see Figure 8c). The first weight loss step, below 120 °C, attributed to the water adsorbed, was a trivial 0.45% weight loss. However, the important weight loss was centered at 250 °C, were the sample lost

**ADVANCED
SCIENCE NEWS**

www.advancedsciencenews.com

**ADVANCED
SUSTAINABLE
SYSTEMS**

www.advsustainsys.com

Pimaric acid   Isopimaric acid   Abietic acid   Dehydroabietic acid   Palustric

**Figure 4.** Schematic of the primary components of silver fir and Rocky mountain fir resins.

circa 80% of its weight (up to 450 °C). A second main decomposition temperature was observed at ≈340 °C, followed by a third considerable weight loss of circa 6.4%. Up to 650 °C. The very last step up to 900 °C showed a minor loss of ≈0.08%, leaving behind a residual weight of circa 14%. The latter value differ nevertheless from the respective one of silver fir for which a 1% charred material was measured at the end of the experiment.

3.4. Dielectric Investigation

Impedance spectroscopy represents a powerful and informative tool used to explain the processes that occur at interfaces between two different materials that lead to changes in physical properties of the system, i.e., crystallographic, electrical, mechanical or even compositional.[46] In our particular interest, impedance spectroscopy helps explaining changes in the electrical properties of the system by studying the effect of polarization on the electrical conductivity variation. Therefore, by performing the conductivity measurement over a wide range of frequencies (i.e., 1 MHz to 1 mHz), impedance spectroscopy offers valuable pieces of information on the different conductive species and pathways. In our particular case in this work, we were interested to see possible relaxation (dome shape on

the graph) of loss angle and sharp increase of capacitance at low frequencies (below 1 Hz), events that are indicative of the presence of mobile ionic species in the dielectric.[47,48,49,50]

We performed dielectric measurements on a thin film of 255 nm thick of silver fir resin spin-coated from a 50 mg ml^{-1} solution concentration in ethanol, and dried on 1 mm wide aluminum electrode in a metal-insulator-metal configuration, with 1 mm wide aluminum also as the top electrode material. We measured the dielectric spectroscopy between 1 MHz and 1 mHz and observed a very uniform capacitance all over the measurement range. Likewise, the loss angle (tangent delta) showed no relaxation behavior over the entire measurement range (see **Figure 9**). Both events are indicative of a very high purity dielectric film, with good dielectric performance. The capacitance and loss angle increased significantly for silver fir only when very low frequencies were reached, i.e., ≈50 mHz or lower. The respective frequency window (i.e., 1 mHz to 50 mHz) is irrelevant for solid state electronics and indeed the OFETs with silver fir dielectric showed no hysteresis in both transfer and output characteristics, as it will be shown in the transistor measurement section. We also measured the impedance spectroscopy on two different solutions of silver fir, in order to assess the resin material stability. The old solution of silver fir resin was produced in October 2017 and the new solution in September 2021, but the two solutions did not originate
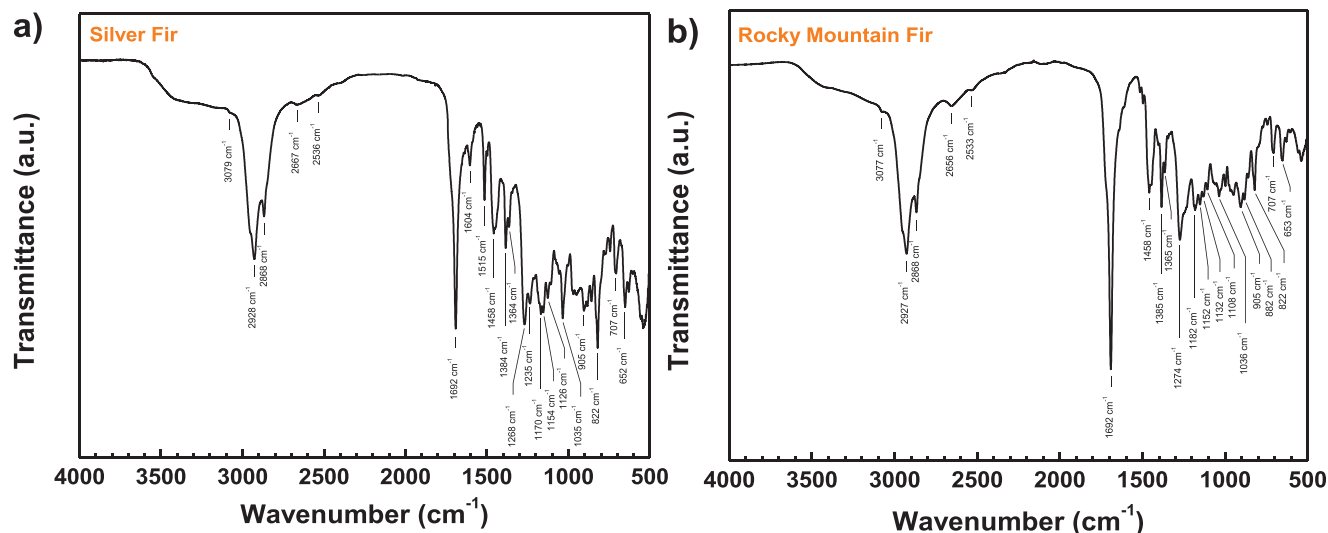
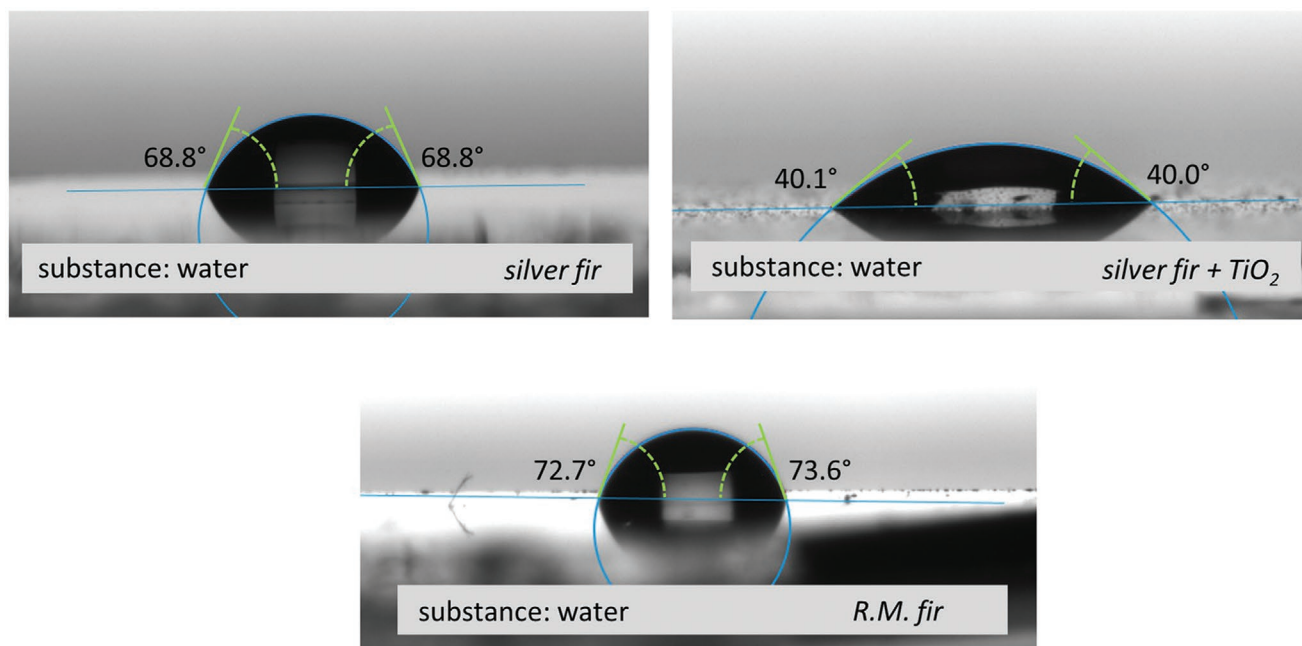**Figure 5.** a) ATR-FTIR spectrum of silver fir resin; b) ATR-FTIR spectrum of Rocky mountain fir resin.
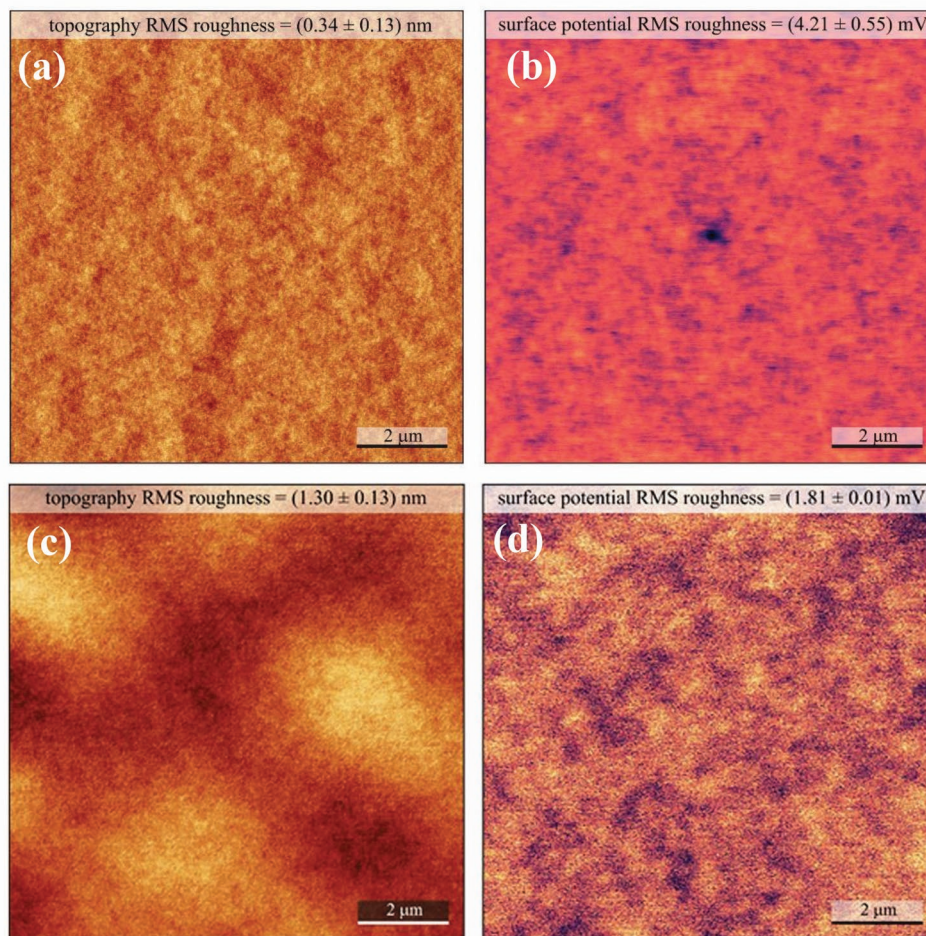
Figure 6. Kelvin probe AFM measurement of a) topography, and b) surface potential of silver fir resin spin-coated on gold electrodes; c) topography and d) surface potential of Rocky mountain fir resin spin-coated on gold electrodes.

from the same resin nugget, but from two different nuggets collected from the same silver fir tree (the "old" resin collected in October 2017 and the "new" resin collected in September 2021 respectively). In the 4 years span, the old solution of silver fir was stored in a closed vial in a laboratory box in ambient air. Both films employed in the dielectric investigation shown here were cast and measured in October 2021. The capacitance and loss angle data of the two MIM structures produced from the two-silver fir solution is shown in Figure 9a) and demonstrate a very good reproducibility. Moreover, we observed that the increase of both capacitance and loss angle at very low frequencies (below 50 mHz) is not due to the aging of the solution, but it is an intrinsic property of the resin itself. From the plotted data of the capacitance at 1 kHz, we extracted a dielectric constant of 4.4 for silver fir. The standard deviation of the 16 samples analyzed in MIM configuration for dielectric constant evaluation was ±0.3. We also performed dielectric measurements on a thin film of ≈60 nm thick of Rocky mountain fir resin from a 20 mg ml^{-1} solution in ethanol, spin-coated and dried on 1 mm wide aluminum electrode in a metal-insulator-metal configuration, with aluminum also as the top electrode material. We measured the dielectric spectroscopy between 10 kHz and 1 mHz and observed a very uniform capacitance

all over the measurement range. Similar to the silver fir resin dielectric, the loss angle (tangent delta) of Rocky mountain fir shows no relaxation behavior over the entire measurement range (see Figure 9c)). Both events are indicative of a very high purity dielectric film, with good dielectric performance. The significant increase of loss angle and capacitance occurs at frequencies below 50 mHz, in a similar fashion to silver fir. This increase may be indicative of the presence of some ionic species inside the resin film, which does not come to a surprise, given the intricate composition of the resin revealed by our materials analysis techniques (GC and HPLC); nevertheless, this increase of both capacitance and loss angle at frequencies below 50 mHz are not influential for the OFET behavior, as can be seen in the transistor section below. From the capacitance of the film at the frequency of 1 kHz, and given the thickness of the film of 60 nm, we calculated a dielectric constant of 4.8 for Rocky mountain fir. The spread of the dielectric constant for the 16 investigated MIM structures was ±0.2.

For the particular case where titania nanoparticles (5 mg ml^{-1} concentration) were added to silver fir solution, we extracted a dielectric constant of 15 at 1 kHz (see Figure 9b)). We investigated also the stability in time of the rocky mountain fir resin and measured the dielectric data for a fresh film, cast from a

**ADVANCED
SCIENCE NEWS**

www.advancedsciencenews.com

**ADVANCED
SUSTAINABLE
SYSTEMS**

www.advsustainsys.com

Figure 7. Top left: Contact angle of silver fir resin with water droplet as displayed in the figure, 68.3° ± 2°. The contact angle of the same resin with diiodomethane (not shown in the figure) was 31.7° ± 0.4°. The deviation of both quantities shows the spread of the measurement values of at least three droplets (left and right). Total surface energy, 50.8 mN/m, divided into a disperse component 43.5 mN m^{-1} and a polar component 7.3 mN m^{-1}; Top right: Contact angle of silver fir resin containing titania insertions with water droplet as displayed in the figure, 40.1° ± 1.8°; Bottom: Contact angle of Rocky mountain fir resin with water droplet as displayed in the figure, 72.7° ± 3.8°. The contact angle of the same resin with diiodomethane (not shown in the figure) was 38.2° ± 2°. The deviation of both quantities shows the spread of the measurement values of at least three droplets (left and right). Total surface energy, 46.9 mN m^{-1}, divided into a disperse component 40.5 mN m^{-1} and a polar component 6.4 mN m^{-1}.
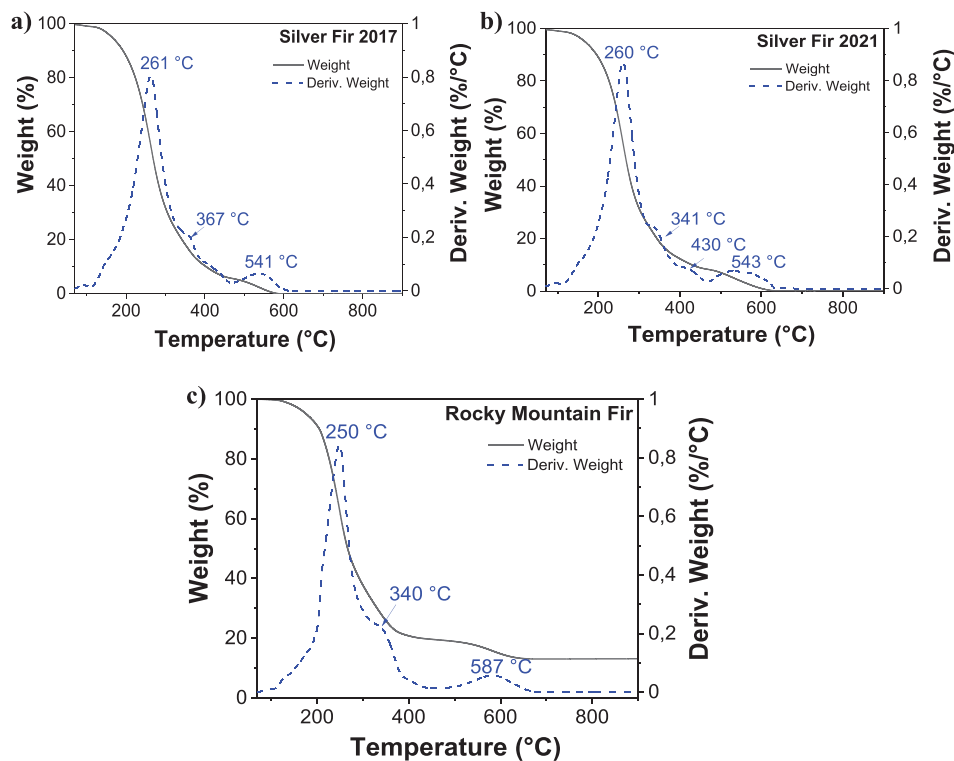
Figure 8. a) Thermogravimetric analysis of the silver fir resin collected in October 2017 and kept in the closed storage vial in the laboratory cabinet all this time, and b) the one collected in September 2021 from the same tree and used immediately for thermogravimetric analysis. The TGA experiment for both samples was carried in October 2021. c) Thermogravimetric analysis of the Rocky mountain fir resin.
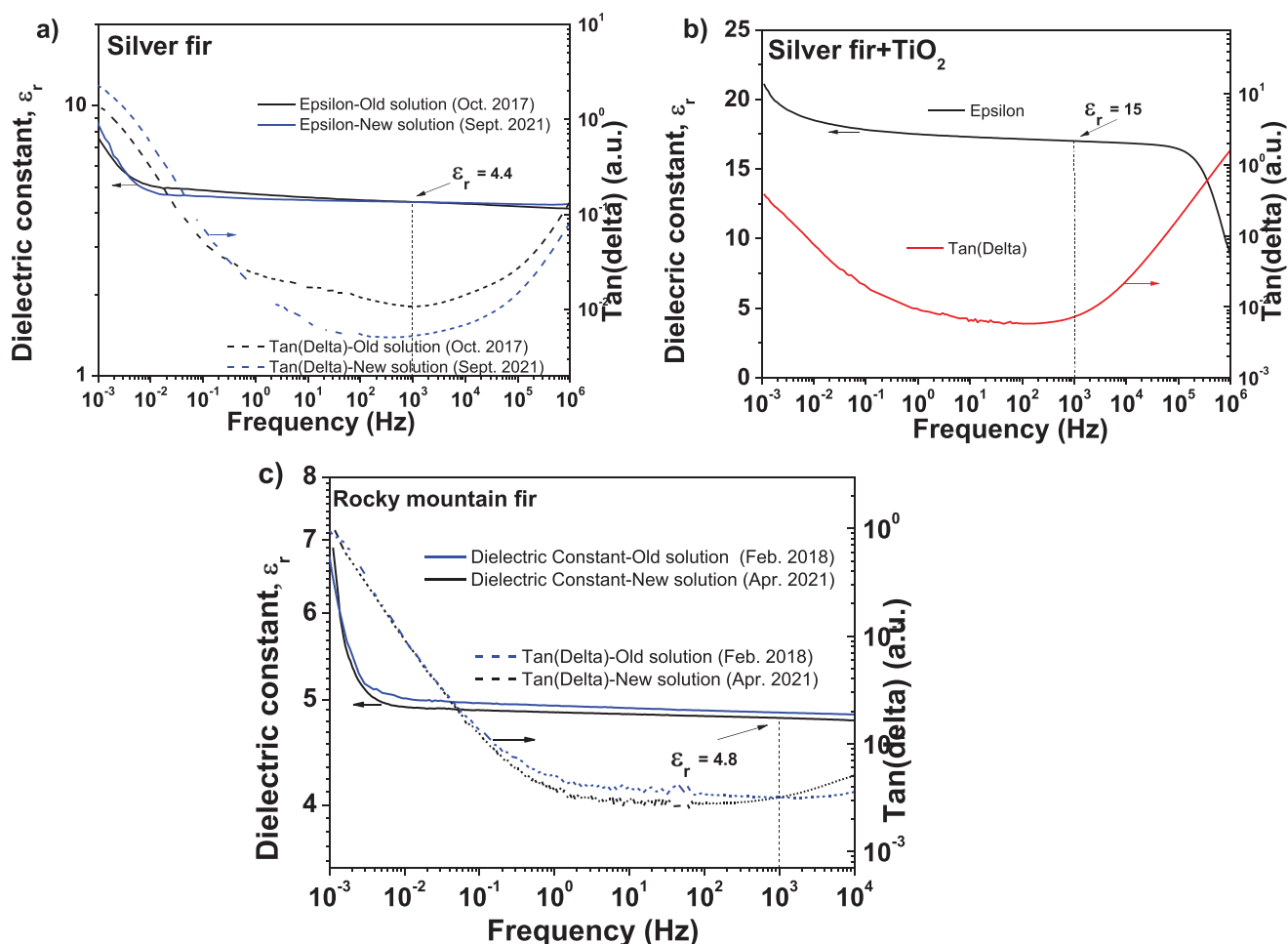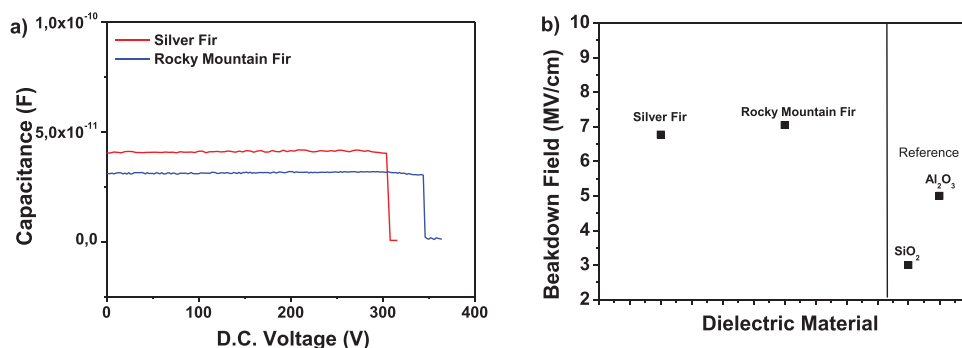
Figure 9. Impedance measurement of a) Silver fir resin; b) Silver fir resin with TiO_2 insertions (in 5 mg ml^{-1} concentration) and c) Rocky mountain fir resin in metal-insulator-metal (MIM) configuration between top and bottom Al electrodes. All resins were solubilized in ethanol and processed in thin film by spin coating.

solution prepared in April 2021 and compared it with the data obtained from a film stemming from the initial solution of the same concentration (20 mg ml^{-1}), prepared in February 2018. Different than in the case of silver fir, here both solutions were prepared from the same Rocky mountain fir nugget that was preserved in laboratory conditions in ambient air. The data presented in Figure 9c) shows an outstanding stability of the dielectric properties of the rocky mountain fir solubilized in ethanol in terms of dielectric constant, purity (absence of ionic movements), and breakdown field.

We cast a film of 449 nm thick silver fir from a 100 mg ml^{-1} concentration solution and performed the breakdown voltage investigation. The resin film broke at 304 V, which translates into a breakdown field of 6.77 MV cm^{-1} for silver fir resin processed from ethanol. The cast film of 60 nm thick Rocky mountain fir (spin-coated from a 20 mg ml^{-1} solution) broke at 40 V, which translates into a breakdown field of 6.6 MV cm^{-1}. We casted also films of rocky mountain fir from a 100 mg ml^{-1} stock solution. One such film had a thickness of 425 nm, and it broke at 304 V, which translates into a breakdown field of 7.15 MV cm^{-1}. Depositing another film from the same 100 mg ml^{-1} stock solution but employing a lower rotation speed of the spin

coater, we generated a rocky mountain fir film with a thickness of 490 nm. The respective film broke at 346 V, which translates into a breakdown field of 7.05 MV cm^{-1}. We believe that the discrepancy in the obtained results (low vs high thicknesses) is due to the error induced by the thin nature of the original film cast from the diluted precursor solution, possibly due to the nonuniformity of the contact electrodes on such thin film or possibly also due to the presence of nanometer size pin-holes. Nevertheless, it seems plausible to consider a breakdown field of ≈7 MV cm^{-1} for Rocky mountain fir. We emphasize nevertheless the high breakdown fields of the two fir resins, taking into consideration the fact that synthetic polymer resins like benzo-cyclobutene (BCB) have a breakdown field or dielectric strength no higher than 4.5 MV cm^{-1}.[51,52] The breakdown field measurement of the two fir resins and its comparison with reference inorganic dielectrics, SiO_2 and Al_2O_3 measured in our laboratories is presented in **Figure 10**.

We investigated complex dielectric properties by ellipsometry for both silver fir and Rocky mountain fir resins (displayed in **Figure 11**) and observed that the two resins have multiple optical transitions in the UV spectral range and are basically transparent within the visible to near infrared range

**ADVANCED
SCIENCE NEWS**

www.advancedsciencenews.com

**ADVANCED
SUSTAINABLE
SYSTEMS**

www.advsustainsys.com

Figure 10. a) Breakdown field measurement for silver fir and Rocky mountain fir resins; b) Silver fir and Rocky mountain fir in comparison in reference to the inorganic dielectric with respect to their breakdown field.

of radiation. For both materials, tail absorptions extend into the visible range giving the two resin a slightly tainted appearance in thick layers. The two fir resins are isotropic, and their real refractive indices range between 1.5 and 1.6, which is similar to the one of float glass. These resins are similar in their thin film appearance, with both films being indistinguishable from one another, while having a pale-yellow color when being either spin coated or doctor bladed on glass substrates.

3.5. Transistor Measurements

We fabricated field effect transistors on both silver fir and Rocky mountain fir resins on 18 nm thin Al_2O_3 films electrochemically grown on the aluminum gate electrodes with pentacene as the organic semiconductor, and gold for the source and drain electrodes. In addition, we also fabricated a stock solution of silver fir containing inorganic nanoparticles. We selected TiO_2 for the respective investigation, and added 5 mg ml^{-1} inorganic filler in the precursor solution of silver fir in ethanol (2 mg ml^{-1}), so that the dielectric layer becomes very thin and thus suitable for the fabrication of low operation voltage OFETs. For the later type of OFETs, no alumina layer was grown on the aluminium gate electrode, so that the film of silver fir containing titania nanoparticles represent the sole dielectric layer. In **Figure 12** the topography of the pentacene semiconductor grown on pure silver fir, on titania containing silver fir resin, and on Rocky mountain fir resin respectively is presented.

The pentacene grains grown on the Al_2O_3 are dentritical and uniform in size. Due to the smooth dielectric surface with RMS roughness (i.e., in the range of 1 nm or below) formed by the employed resin solutions (plain silver fir, silver fir with TiO_2 insertions and plain Rocky mountain fir), the pentacene grains grew in aggregates of grains with sizes larger than 1 µm (see Figure 12). The largest size of pentacene grains was found on the silver fir solution with TiO_2 nanoparticles where grains of up to 5 µm were observed, as shown in Figure 12b)). Rocky mountain fir allowed pentacene to grow in grain sizes between 1 µm and 3 µm, in a striking similarity to silver fir. Both pentacene films grown on plain silver fir and Rocky mountain fir solutions shown in Figure 12a,c) show secondary nucleation of new grains on top of the underlying coalesced pentacene grains. Interestingly though, we did not observe this event for pentacene films grown on the titania containing silver fir film.

The architecture of the OFET device employed all throughout this work involved a staggered bottom gate-top contact design (see Figure 2). We define the transistor parameters as follows: the ON/OFF ratio is the ratio between the current in no conduction mode and the maximum current attained in the operation regime of the device. The threshold voltage (V_{th}) is determined as the intercept on the horizontal axis of the tangent drawn to the linear part of the square root of the I_{ds} versus V_{gs} line in the saturation regime of the transistor. There, I_{ds} stands for the source-drain current and V_{gs} for the gate-source voltage. The field effect mobility of the semiconductor in the saturation regime is extracted from the equation:
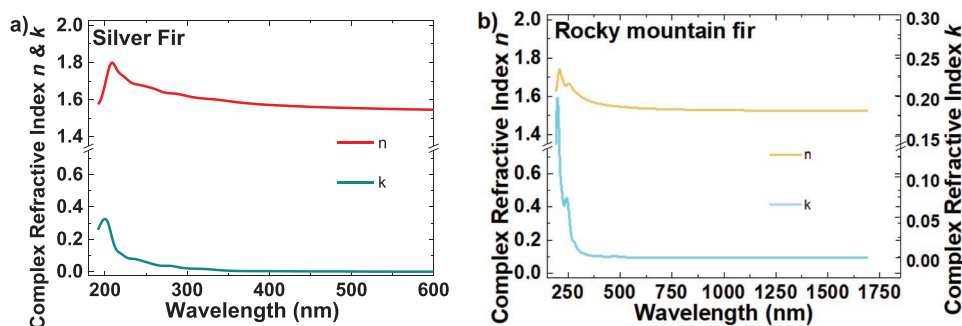
Figure 11. a) Complex refractive index of silver fir resin; b) complex refractive index of Rocky mountain fir resin.

**ADVANCED
SCIENCE NEWS**

www.advancedsciencenews.com

**ADVANCED
SUSTAINABLE
SYSTEMS**

www.advsustainsys.com
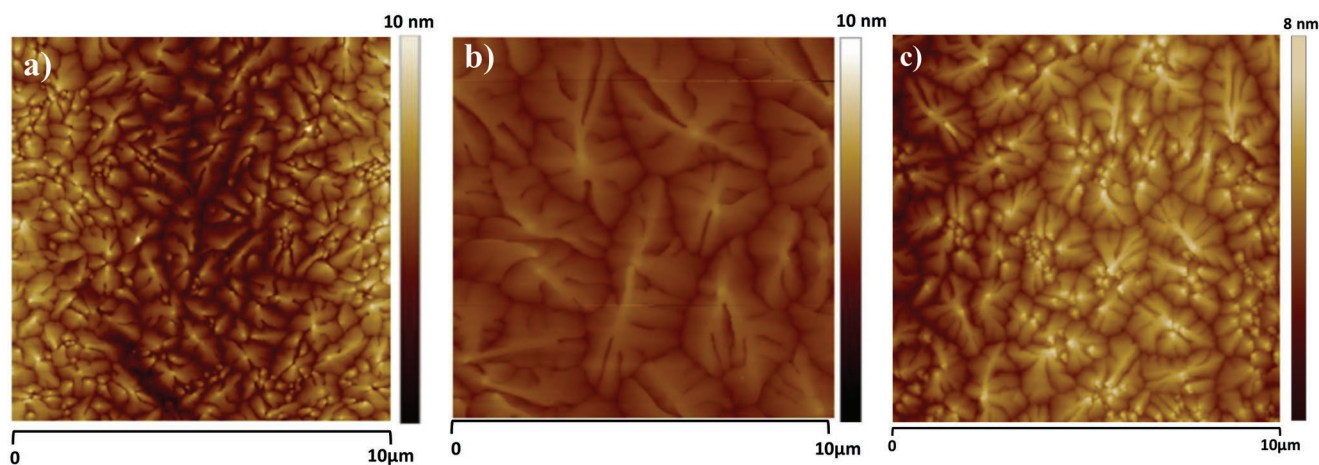
Figure 12. AFM scan of pentacene on (a) on plain silver fir-device presented in Figure 8a); (b) silver fir with TiO_2 insertions-device presented in Figure 15a); (c) plain Rocky mountain fir dielectric channel of the devices presented in Figure 8b).

$$I_{ds,sat} = (W/2L) C_{od} \mu_{sat} (V_{gs} - V_{th})^2 \qquad (7)$$

The subthreshold swing (S_{sw}) is the inverse of the subthreshold slope (S_{sl}), and can be extracted from the equation:

$$S_{sw} = 1/S_{sl} = dV_{gs}/d(\log I_{ds}) \qquad (8)$$

The subthreshold swing indicates how fast the OFET device switches form the OFF to the ON state. With this respect, a large value of the subthreshold swing indicates a large concentration of shallow traps, i.e., a slow and nonsharp turn-on region. For mobility calculations, for particular cases of OFET devices where a straight line is not an accurate fit to the sqrt(I_{ds}), we fitted the line at higher gate voltages. The start and end points of the subthreshold swing were determined from the best straight line fit to a gate voltage interval on the $\log(I_{ds})$ versus V_{gs} plot for lower gate voltages than the threshold voltage, as thoroughly explained in the review article of Newman et al.[53]

The normalized subthreshold swing (S_{sn}) is given by the equation:

$$S_{sn} = S_{sw} \times C_{0d} \qquad (9)$$

The normalized subthreshold swing is a more convenient method of comparison of the performance of organic semiconductors in OFET devices, when deposited on various dielectrics, or on dielectrics of different thicknesses.[53] In the equations depicted above, $I_{ds,sat}$ represents the transistor drain-source current in the saturation regime, W and L are the geometric factors of the transistor channel (i.e., length, L and width, W; in our case 2 mm and 35 µm respectively), C_{0d} is the specific capacitance of the dielectric (i.e., in our case the combo layer inorganic, Al_2O_3 and organic, resin), μ_{sat} is the field effect mobility of the organic semiconductor in the saturation regime, V_{gs} and V_{th} are the gate and the threshold voltages respectively, and S_{sw} is the subthreshold swing, expressed in volts per decade of current.

We fabricated OFETs with silver fir as a capping layer for the electrochemically grown Al_2O_3 dielectric. The solution of silver

fir had a concentration of 20 mg ml^{-1} in ethanol. The thickness of the aluminum oxide dielectric, i.e., ≈18 nm was dictated by the anodization voltage that was kept constant at 10 V during the process. The OFET characteristics of silver fir resin showed hysteresis-free behavior both in transfer and output characteristics (see **Figure 13**a–c). The behavior of the combined inorganic-organic gate dielectric layer was characterized by a very low leakage in the range of 10–100 pA all throughout the measurement range (i.e., 4 V to −8 V, Figure 13a). The calculated semiconductor mobility was ≈0.04 cm^2 Vs^{-1}. The subthreshold swing of device was 1.2 V dec^{-1}, and the normalized subthreshold swing was 38.6 VnF cm^{-2} dec^{-1}. A characteristic of silver fir resin was the relatively high OFF level in the transfer characteristics, which we attribute to the tendency of the dielectric material for charging the semiconductor in the OFF state.

We fabricated also field effect transistors on Rocky mountain fir resin-capped aluminum oxide gate electrode and pentacene semiconductor. The devices were capped by gold source and drain electrodes. The transfer and output characteristics of the respective devices are presented in Figure 13b,d. Different than in the case of silver fir, we explored the possibility to fabricate low voltage operating devices, by halving the anodization voltage required by the electrochemically grown process of aluminum oxide from 10 V in case of silver fir to 5 V in case of Rocky mountain fir. We also diluted eight times the Rocky mountain fir solution, and cast the respective capping layer film of Rocky mountain fir film from a 2.5 µg ml^{-1} stock solution. The anodization voltage employed in the electrochemical growth process of aluminum oxide is very important parameter in the operation of the field effect transistor, because, the unpassivated oxide film can withstand in the OFET measurement an applied gate voltage roughly half the value of the voltage used in the anodization process (i.e., ≈V_{gs} = −5 V for the 10 V anodization voltage of silver fir and ≈V_{gs} = −2.5 V for the respective value of 5 V anodization voltage for Rocky mountain fir). The fact that our devices withstand higher voltages without any visible leakage, i.e., spike in the I_{gs} current, (i.e., −8 V for silver fir and −3 V for Rocky mountain fir) is a direct consequence of the robustness of the two
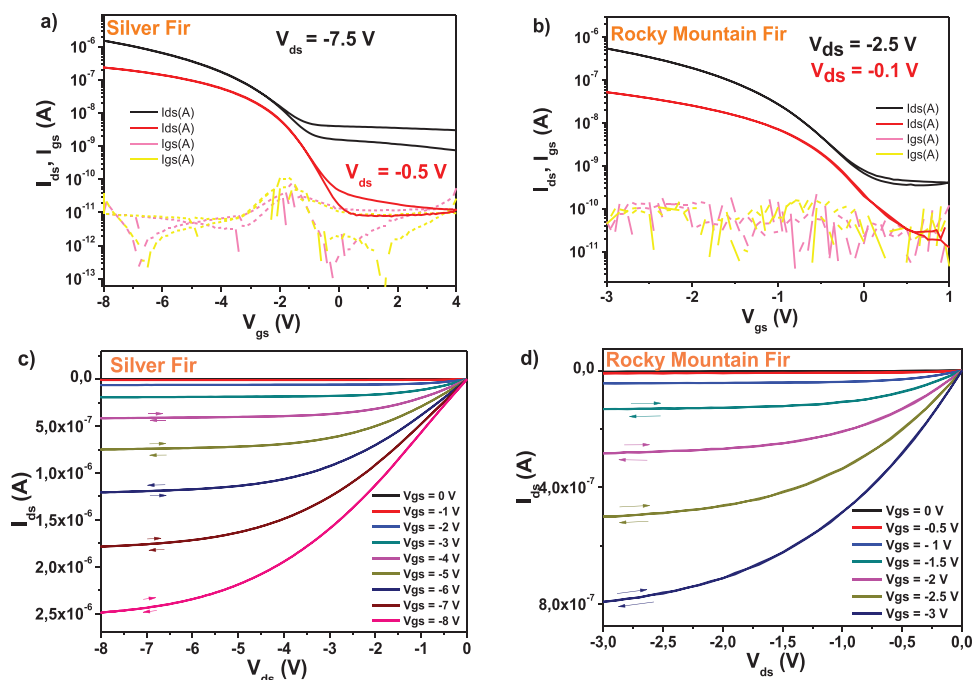
Figure 13. Transistor characteristics of silver fir and Rocky mountain fir resins as capping layers for Al_2O_3 dielectric with pentacene semiconductors. a) and c) transfer and output characteristics for pentacene semiconductor on silver fir; specific Capacitance: 32.22 nF cm^{-1}.[2] Field effect mobility is 4×10^{-2} cm^2 Vs^{-1}; b) and d) transfer and output characteristics for pentacene semiconductor on Rocky mountain fir, specific Capacitance: 72.77 nF cm^{-1}.[2] Field effect mobility is 4×10^{-2} cm^2 Vs^{-1}. The difference in operating voltages of the devices with silver fir and Rocky mountain fir stems from the difference in thickness of the Al_2O_3 layer in the two cases, given by a different anodization potential used in the electrochemically growth process of aluminum oxide. Silver fir OFET was cast from a 20 mg/ml solution in ethanol, whereas the Rocky mountain fir OFET from a 2.5 mg ml^{-1} solution in ethanol. Measured thicknesses of the resins layers: ≈50 nm for silver fir and ≈10 nm for Rocky mountain fir.

resins employed as capping layers. We stopped scanning to higher voltages for the two types of devices because other devices fabricated in the same batch started to leak at applied voltages higher than 8 V for silver fir or 3 V for Rocky mountain fir and pentacene semiconductor. We concluded that the two employed gate voltages were optimal for the thickness of the two capping layer resins stemming from the 20 µg ml^{-1} and 2.5 µg ml^{-1} concentration resin solutions (i.e., ≈50 nm for silver fir and ≈10 nm for Rocky mountain fir). In a similar case with the silver fir devices, also rocky mountain fir generated an interface to the organic semiconductor that had characteristic a high OFF level of the source-drain current when devices were measured in transfer mode. For pentacene, the respective level was in the range of 0.6 nA, and the device was hysteresis free in both transfer and output characteristics. The calculated field effect mobilities of the latter device was situated in the same range with the one of silver fir, i.e., ≈0.04 cm^2 Vs^{-1}, with a sub-threshold swing of 0.6 V dec^{-1}, and a normalized subthreshold swing of ≈43.5 VnF cm^{-2} dec^{-1}. In the simplest theory, the subthreshold swing roughly scales with the inverse of the specific capacitance of the dielectric layer ($1/C_{od}$), as demonstrated by Zirkl et al.,[54] meaning that the normalized subthreshold swing is proportional to the interface trap density. Given the fact that the OFETs fabricated with the two resins employed here have comparable to one another normalized subthreshold swing (i.e., 38.6 VnF cm^{-2} dec^{-1} and 43.5 VnF cm^{-2} dec^{-1}), the interface trap density of the two materials is similar, or in other words, the two dielectrics offer competitively analogous interfaces for the charge transport.

Another type of measurement that we performed for the two resins was the consecutive scanning of the transfer characteristics. Although one can extend indefinitely this type of test, i.e., scanning for a specific amount of time, say 12 or 24 hours, or even a specific number of cycles, 1000 or 10 000 cycles (see[55] and the citations therein, and considering that there is by now no accepted norm in the scientific community for this type of test), sometimes a limited number of cycles is enough to give an impression over the stability of the semiconductor channel during consecutive scanning. We observed that the threshold voltage moved by 8 mV after six consecutive scans of silver fir OFET, while the transfer characteristics showed a negligible increase of the OFF level of the device, alongside the insignificant (≈1.2%) increase in ON current, from 1.133×10^{-6} A to 1.142×10^{-6} A. The Rocky mountain fir device scanned consecutively for 8 readouts and behaved in a similar fashion. The shift of threshold voltage was only 3 mV (**Figure 14**b).

Between the two resins investigated in this work we selected one of them (silver fir) and investigated the OFET characteristics of the device fabricated with an insertion of inorganic nanoparticles in the resin layer. We used titania for the respective investigation (i.e., the main reason for this choice was its biocompatibility and very low toxicity), and added the inorganic filler in a 5 mg ml^{-1} concentration in the precursor solution of silver fir in ethanol that had silver fir in a concentration of
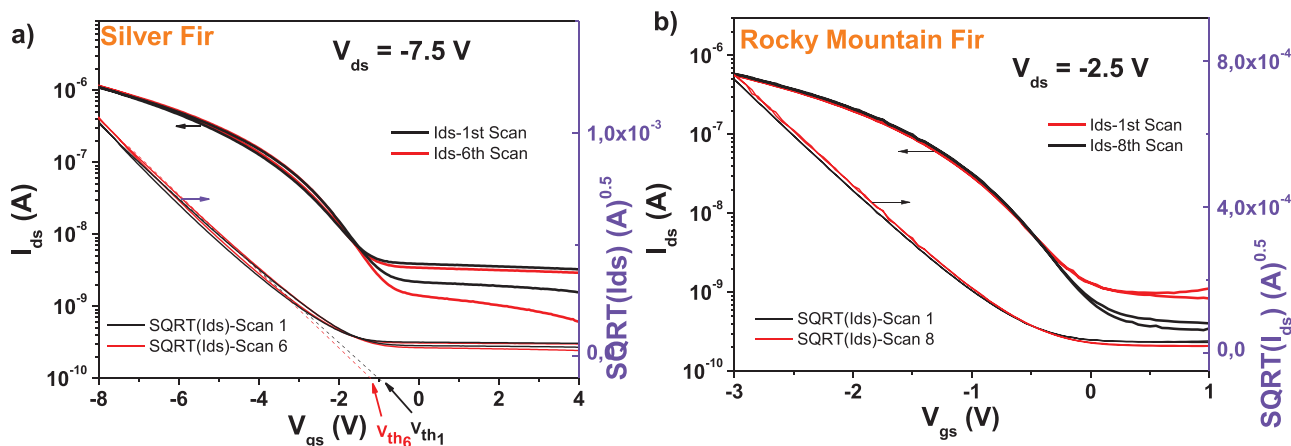
Figure 14. a) Consecutive transfer measurement stability for silver fir resin dielectric with pentacene semiconductor; b) Consecutive transfer measurement stability for Rocky mountain fir resin dielectric with pentacene semiconductor.

2 mg ml^{-1}. We employed for this test a diluted silver fir solution (2 mg ml^{-1}), so that the dielectric layer will become very thin after spin-coating and afford therefore the fabrication of low-voltage operation OFET. We compared the OFET characteristic of two independent devices: one stemming from a plain silver fir solution of 2 mg ml^{-1} in ethanol and the other from a 2 mg ml^{-1} silver fir solution in ethanol containing 5 mg ml^{-1} inorganic TiO_2 filer (see **Figure 15**a). It is obvious that plain silver fir in such a thin layer configuration is a little bit leaky as a dielectric, but nonetheless, the titania particles help improve its insulator properties. In this comparative study, we cast the two dielectric films (silver fir and silver fir with

titania insertions) directly on aluminum gate, therefore without aluminum oxide gate dielectric (Figure 15a). The thickness of the plain silver fir resin film on aluminum gate dielectric was in the range of 28 nm, whereas the thickness of the film of silver fir with titania nanoparticles was in the range of 20 nm. The output characteristics of these devices are displayed in Figure 15b,c. Both devices (plain silver fir and silver fir + titania insertions respectively) worked at 1 V, but despite the higher current recorded for the inorganic filler-based device, due to the higher specific capacitance of the titania-based device, the field effect mobility of the two devices were not much different, both being in the range of 0.04 cm^2 Vs^{-1}, although a cham-
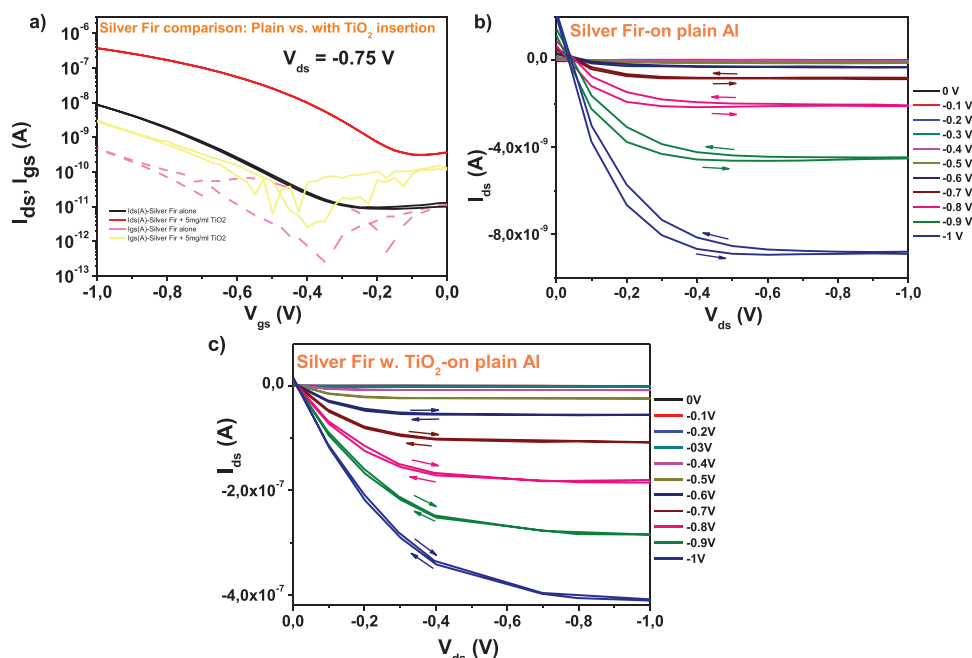

Figure 15. Low voltage operating devices on plain aluminum gate electrode: a) comparison of transfer characteristics of OFETs with plain silver fir layer and silver fir with insertion of titania particles; Specific capacitance: 132.65 nF cm^{-2} for plain silver fir and 714.59 nF cm^{-2} for silver fir with titania nanoparticles. Field effect mobility: 4×10^{-2} cm^2 Vs^{-1} for plain silver fir dielectric and 5×10^{-2} cm^2 Vs^{-1} for silver fir with titania insertions; b) output characteristics of plain silver fir film; c) output characteristics of silver fir film with titania insertion.

**ADVANCED
SCIENCE NEWS**

www.advancedsciencenews.com

**ADVANCED
SUSTAINABLE
SYSTEMS**

www.advsustainsys.com

pion device of titania containing silver fir dielectric recorded a field effect mobility of 0.05 cm^2 Vs^{-1}. Interestingly, a larger pentacene grain size detected on the titania containing silver fir dielectric surface (see Figure 12) did not lead to a higher charge carrier mobility. Nevertheless, the rationale for performing this study was double fold: 1) to show that low operating voltage OFETs can be obtained for standalone resin films without aluminum oxide, and 2) to show the immense potential of the system natural resin + inorganic fillers. Our goal was achieved but without a doubt more insight and optimization will be needed in order to reach an acceptable level of performance in alumina-free resin dielectric systems. The subthreshold swing of the two type of fabricated OFETs in this comparison study (plain silver fir and silver fir with titania on plain aluminum gate) was in the same range: 0.25 V dec^{-1}. for the first and 0.2 V/dec. for the latter. Nevertheless, the normalized subthreshold swing was much smaller for plain silver fir, i.e., 33.06 VnF cm^{-2} dec^{-1} versus 142.23 VnF cm^{-2} dec^{-1} for the device containing titania nanoparticles. This large difference in a normalized subthreshold swing is translated into a much higher interface trap density for the device containing nanoparticles, due to its higher polarizability and can explain why the mobility of the two devices is virtually the same despite larger grain size of the pentacene grown on titania containing silver fir, as shown in Figure 12b).

Finally, we performed bias stress measurement of the OFETs used for transfer and output characteristics with pentacene semiconductor for both silver fir and Rocky mountain fir-based devices spin-coated on Al$_2$O$_3$ dielectrics. We stressed the devices at the maximum voltage used for transfer measurement, i.e., −8 V for silver fir and −3 V for RM fir respectively-in reality we used for this test the same devices reported for OFET characteristics in Figure 13, while keeping both these drain and gate voltages constant for 12 h stress time. We measured the transfer characteristic at the beginning of the test, as well as immediately after releasing the electrical stress, and observed that the silver fir OFET device displayed a ≈91% retention of the initial source-drain current after bias stress test was concluded, while the Rocky mountain fir retained a more robust ≈96% of the original I_{ds} current before the bias stress (**Figure 16**a,b). We continued to measure the recovery curve of both devices with 5 minutes time delay between measurements (i.e., one full OFET transfer characteristic measurement takes ≈30 s), but for simplicity and the avoidance of cluttering the graph, we show here only the transfer curve where the full or nearly full recovery was measured. In the case of silver fir, the ON level of the drain current, as well as the threshold voltage, almost fully recovered in 2 hours relaxation after the bias stress time of 12 h. The device offered also a good stability with respect to this type of test, where only 5 nA upshift of the OFF level
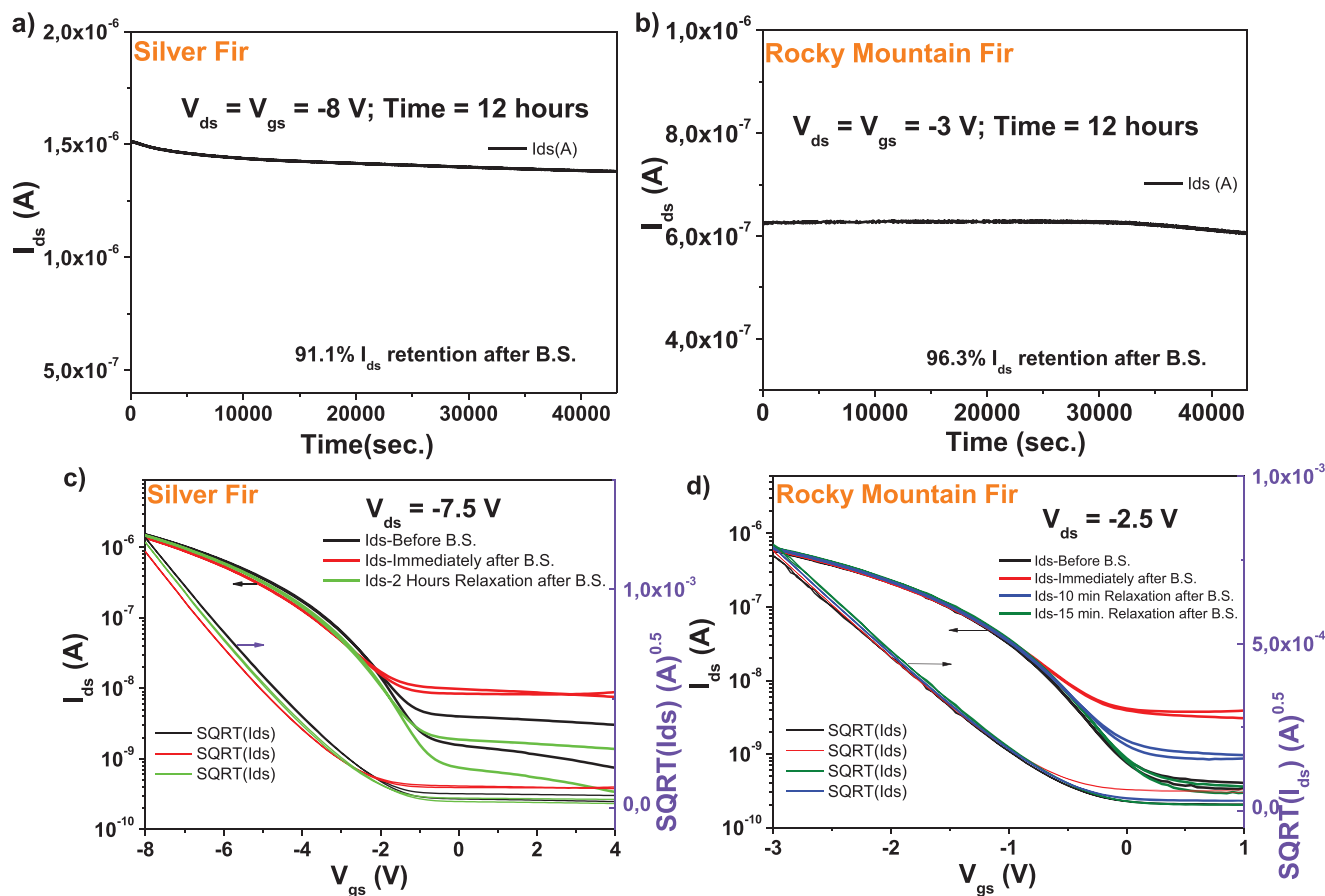
Figure 16. a) Bias stress and b) Recovery after bias-stress of the silver fir OFET characteristics with pentacene semiconductor; c) Bias stress and d) Recovery after bias-stress of the Rocky mountain fir OFET characteristics with pentacene semiconductor.

Table 4. Dielectric and semiconductor properties for the fabricated OFETs with pentacene.

	Surface property			Dielectric property			Semiconductor performance in OFET with AlOx + resin					
							OFET parameters			Bias Stress		
Dielectric	Roughness (nm)/ Contact potential difference (mV)	Contact angle (deg.)	Surface Energy [mN/m] (disperse/ polar)	Dielectric constant (a.u.)	Loss Angle at 10^{-2} Hz (a.u.)	Breakdown field [MV cm^{-1}]	Mobility [cm^2 Vs^{-1}]	S_{sw} [V dec^{-1}]	S_{sn} [VnF cm^{-2} dec^{-1}]	Time [h])]/ Voltage [V]	I_{ds} retention [%]	Recovery time [min]
R.M. fir	1.3/1.81	71.8	40.5 6.4	4.8 ± 0.2	0.1	7	4 × 10^{-2}	0.6	43.5	12/(−3)	96.3	15
Silver fir	5.1 / 4.72	67.3	43.5 7.3	4.4 ± 0.3	0.65	6.77	4 × 10^{-2}	1.2	38.6	12/(−8)	91.1	120

was observed from the start to the finish of the 12 hours bias stress, without any major change of threshold voltage or ON current (Figure 16c). Rocky mountain fir resin fully recovered within a record 15 min of relaxation after the completion of the bias stress (Figure 16d), while also showing impressive robustness with respect to threshold voltage shift compared before and after bias stress. The only drawback of the sample during the bias stress was the ≈10 nA upshift of the OFF level. Nevertheless, the OFF level fully recovered within 15 min of relaxation time after completion of the bias stress, which makes the respective device one of the most performant devices ever reported for bias stress.[55,56,57,58,59]

The OFETs and bias stress parameters are summarized in **Table 4**, while the composition of the two resins is displayed in Tables 1, 2, and 3.

To summarize, the two investigated fir resin-based dielectrics have exceptional dielectric properties, including here virtually frequency-independent dielectric constants and low relaxation (loss angle) values over a wide frequency range, and high breakdown fields in the range of 7 MV cm^{-1}. They form a smooth surface when applied on anodic Al$_2$O$_3$ thus inducing a course pentacene semiconductor morphology with grain sizes higher than 1 µm upon thermal evaporation. When integrated as a gate dielectric in pentacene-based OFETs these excellent dielectric properties translate into totally hysteresis-free and reproducible characteristics with exceptional bias stress stability and very short recovery time not often observed in transistors deploying the typical inorganic or polymeric gate dielectrics. The respective devices show very good stability in terms of electrical stressing (bias stress), with high I_{ds} retention surpassing 90%, and recovery times after bias stress in tens of minutes to a couple of hours. The above-mentioned accolades with respect to bias stress places these systems (i.e., pinaceae (fir) resins-pentacene) among the best stable OFET devices ever reported. The reason for the hysteresis-free behavior may be a specific reorganization process that occurs in the dielectric during the film casting process and its surface to the semiconductor molecules. In this process, the resin layer surface is composed of free, unconnected molecules of the components of the particular resin with a large supply of free surface energy. This high surface energy allows the resin molecules to interact strongly with the molecules deposited on the respective layer, in our case the semiconductor molecules, pentacene. We argue that this event might explain the good behavior of the dielectric resin layer

in organic field-effect transistor performance with respect to no hysteresis occurrence between forward and reverse scans. Although it will be hardly possible to identify the unique constituents of the resins that are responsible for this event, especially due to the intricate composition of the respective layers, the observations stemming from this work are in line with the ones reported by us previously for Shellac, an animal resin, for which virtually hysteresis-free OFET devices were fabricated.[60] The charge carrier mobilities of the fir resin-based OFETs are comparable, with values in the range of 4 × 10^{-2} cm^2 Vs^{-1}, as is also the normalized subthreshold swing values which lies for both resins in the range of 40 VnF cm^{-2} dec^{-1}, give or take. A significantly higher value of normalized subthreshold swing, of ≈142 VnF cm^{-2} dec^{-1}. was recorded for the device containing titania nanoparticles embedded in the silver fir gate dielectric. This might be due a rather high interface trap density in the latter device. However, as they obviously do not contribute to hysteresis, these interface traps seem to originate from deeper states in the band gap where trapped charges cannot be released by the operation voltages easily.

The stability of the resins themselves in solid state and solubilized form in ethanol is also outstanding, with no sizable difference in dielectric behavior over prolonged storage of at least 4 years. This stability might be of major relevance for long-term storage and control of production, transportation, and future applications of renewable resources, all these factors being of paramount importance for reaching sustainability in electronics manufacturing.

Moreover, we demonstrated the versatility of the two fir resins: they are excellent insulators, working either as standalone dielectrics in OFETs, or in combination with aluminum oxide or possibly any other oxide inorganics as capping layers. The film forming abilities for fir resins is impressive too, with roughness of the films in the range of 1–5 nm. Importantly, their surface potential, as revealed by the KPFM investigation is one order of magnitude lower than the respective values of Al$_2$O$_3$ or SiO$_2$. The ease of processability of the fir resins is breathtaking, requiring simply solubilization in pure ethanol and a filtration through a hydrophilic paper. When heated at ≈50 °C while stirring the resin solution with a magnet, the full solubility occurs within 10–15 min. The cost of production of these materials is very low, if one considers the time and effort to collect them from the host trees, and then to turn them into their soluble form in ethanol as exemplified above. Their

**ADVANCED
SCIENCE NEWS**

www.advancedsciencenews.com

**ADVANCED
SUSTAINABLE
SYSTEMS**

www.advsustainsys.com

deposition technique can be either spin coating (employed in this work), doctor blading, dip-coating, or even spray coating for large area industrial fabrication. The temperature used for drying the films is also moderate, i.e., 80 °C, the temperature employed here; however, we saw no difference of the quality of the dielectric even when temperatures of 70 °C were employed.

4. Conclusions

The combined results presented in this manuscript suggest that the two fir resins stemming from pinaceae trees (needle type of leaves) are promising candidates for the development of sustainable electronic devices. Several demonstrations and ideas to pursue for future research have been offered here, suggesting that fir resins represent a class of high-quality dielectrics displaying the appealing characteristics of minimal toxicity towards humans and the environment, coupled with robust dielectric characteristics and resistance to degradation in air after prolonged storage, and under electrical stress in electronic devices.

All these considered, the two fir resins investigated in this study are viable alternatives for the fabrication of sustainable, "green" electronics, when all the aspects are fully accounted for. With this respect, factors like origin and wide availability, price of the material, cost of production, toxicity, biocompatibility, biodegradability, and finally the most important aspect, its ultimate performance, and stability-reliability in practical devices have to be wholly considered if the ultimate target is the development of sustainable electronics or sensing systems. Silver fir and Rocky mountain fir resins score high on all these above-mentioned aspects and are a class of dielectric materials to carefully consider for further studies.

[1] P. Georgiadis, M. Besiou, *Sustainability* **2009**, *1*, 722.
[2] T. G. Gutowski, M. S. Branham, J. B. Dahmus, A. J. Jones, A. Thiriez, D. P. Sekulic, *Environ. Sci. Technol.* **2009**, *43*, 1584.
[3] E. Williams, *Environ. Sci. Technol.* **2004**, *38*, 6166.
[4] R. García-Valverde, J. A. Cherni, A. Urbina, *Prog. Photovoltaics* **2010**, *18*, 535.
[5] K. Schischke, N. F. Nissen, M. Schneider-Ramelow, *MRS Commun.* **2020**, *10*, 69.
[6] J. R. Sheats, *J. Mater. Res.* **2004**, *19*, 1974.
[7] H. J. Jina, S. H. Leeb, T. H. Kim, J. Park, H. S. Song, T. H. Park, S. Hong, *Bios. Bioelectron.* **2012**, *35*, 335.
[8] S. H. Lee, M. Lee, H. Yangad, Y. Cho, S. Hong, T. H. Park, *Biosens. Bioelectron.* **2020**, *154*, 112071.
[9] M. Gamella, N. Guz, J. M. Pingarrón, R. Aslebagh, C. C. Darie, E. Katz, *Chem. Commun.* **2015**, *51*, 7618.
[10] P. Meredith, C. Bettinger, M. Irimia-Vladu, A. Mostert, P. Schwenn, *Rep. Prog. Phys.* **2013**, *76*, 034501.
[11] D. K. Khatu, N. P. M. Joseph, R. G. Khandelwal, A. N. Rao, S. J. Kim, *Mater. Today* **2021**, *20*, 100679.
[12] S. Appusamy, S. Krishnan, M. Gopikrishna, S. Raman, *J. Electron. Mater.* **2021**, *50*, 1893,.
[13] S. Xu, A. Jayaraman, J. A. Rogers, *Nature* **2019**, *571*, 319.
[14] H. U. Chung, B. H. Kim, J. Y. Lee, J. Lee, Z. Xie, E. M. Ibler, K. H. Lee, A. Banks, J. Y. Jeong, J. Kim, C. Ogle, D. Grande, Y. Yu, H. Jang, P. Assem, D. Ryu, J. W. Kwak, M. Namkoong, J. B. Park, Y. Lee, D. H. Kim, A. Ryu, J. Jeong, K. You, B. Ji, Z. Liu, Q. Huo, X. Feng, Y. Deng, Y. Xu, et al., *Science* **2019**, *363*, eaau0780.
[15] A. A. Kumar, J. W. Hennek, B. S. Smith, S. Kumar, P. Beattie, S. Jain, J. P. Rolland, T. P. Stossel, C. Chunda-Liyoka, G. M. Whitesides, *Angew. Chem., Int. Ed.* **2015**, *54*, 5836.
[16] L. M. Dumitru, M. Irimia-Vladu, N. S. Sariciftci, *Compr. Anal. Chem.* **2016**, *74*, 247.
[17] M. Irimia-Vladu, *Chem. Soc. Rev.* **2014**, *43*, 588.
[18] K. Bazaka, M. V. Jacob, K. Ostrikov, *Chem. Rev.* **2016**, *116*, 163.
[19] L. Wang, D. Chen, K. Jiang, G. Shen, *Chem. Soc. Rev.* **2017**, *46*, 6764.
[20] D. Martin, *Nat. Mater.* **2007**, *6*, 626.
[21] D. Bennet, S. Kim, *J. Mater. Sci.* **2011**, *46*, 4723.
[22] V. Lundin, A. Herland, M. Berggren, E. W. H. Jager, A. I. Teixeira, *PLoS One* **2011**, *6*, e18624.
[23] D. Khodagholy, T. Doublet, M. Gurfinkel, P. Quilichini, E. Ismailova, P. Leleux, T. Herve, S. Sanaur, C. Bernard, G. G. Malliaras, *Adv. Mater.* **2011**, *23*, H268.
[24] D. H. Kim, N. Lu, R. Ma, Y.-S. Kim, R.-H. Kim, S. Wang, J. Wu, S. M. W. H. Tao, A. Islam, K. J. Yu, T.-il Kim, R. Chowdhury, M. Ying, L. Xu, M. Li, H.-J. Chung, H. Keum, M. McCormick, P. Liu, Y.-W. Zhang, F. G. Omenetto, Y. Huang, T. Coleman, J. A. Rogers, *Science* **2011**, *33*, 838.
[25] C. J. Bettinger, Z. Bao, *Adv. Mater.* **2010**, *22*, 651.
[26] M. Irimia-Vladu, P. A. Troshin, M. Reisinger, L. Shmygleva, Y. Kanbur, G. Schwabegger, M. Bodea, R. Schwödiauer,

A. Mumyatov, J. W. Fergus, V. F. Razumov, H. Sitter, N. S. Sariciftci, S. Bauer, *Adv. Funct. Mater.* **2010**, *20*, 4069.

[27] S.-W. Hwang, H. Tao, D.-H. Kim, H. Cheng, J.-K. Song, E. Rill, M. A. Brenckle, B. Panilaitis, S. M. Won, Y.-S. Kim, Y. M. Song, K. J. Yu, A. Ameen, R. Li, Y. Su, M. Yang, D. L. Kaplan, M. R. Zakin, M. J. Slepian, Y. Huang, F. G. Omenetto, J. A. Rogers, *Science* **2012**, *337*, 1640.

[28] D.-H. Kim, J. Viventi, J. J. Amsden, J. Xiao, L. Vigeland, Y.-S. Kim, J. A. Blanco, B. Panilaitis, E. S. Frechette, D. Contreras, D. L. Kaplan, F. G. Omenetto, Y. Huang, K. C. Hwang, M. R. Zakin, B. Litt, J. A. Rogers, *Nat. Mater.* **2010**, *9*, 511.

[29] C. Schwarzinger, *J. Anal. Appl. Pyrolysis* **2003**, *68-69*, 137.

[30] I. Pastorova, K. J. van der Berg, J. J. Boon, J. W. Verhoeven, *J. Anal. Appl. Pyrolysis* **1997**, *43*, 41.

[31] Y. Udum, P. Denk, G. A. Workneh, D. H. Apaydin, A. Nevosad, C. Teichert, M. S. White, N. S. Sariciftci, M. C. Scharber, *Org. Electron.* **2014**, *15*, 997.

[32] L. A. Majewski, M. Grell, S. D. Ogier, J. Veres, *Org. Electron.* **2003**, *4*, 27.

[33] C. Yumusak, N. S. Sariciftci, M. Irimia-Vladu, *Mater. Chem. Front.* **2020**, *4*, 3678.

[34] M. Irimia-Vladu, P. A. Troshin, M. Reisinger, G. Schwabegger, M. Ullah, R. Schwödiauer, A. Mumyatov, M. Bodea, J. W. Fergus, V. F. Razumov, H. Sitter, S. Bauer, N. S. Sariciftci, *Org. Electron.* **2010**, *11*, 1974.

[35] A. I. Mardare, M. Kaltenbrunner, N. S. Sariciftci, S. Bauer, A. W. Hassel, *Phys. Status Solidi A* **2012**, *209*, 813.

[36] M. Kaltenbrunner, T. Sekitani, J. Reeder, T. Yokota, K. Kuribara, T. Tokuhara, M. Drack, R. Schwö¨diauer, I. Graz, S. Bauer-Gogonea, S. Bauer, T. Someya, *Nature* **2013**, *499*, 458.

[37] G. Schwabegger, M. Ullah, M. Irimia-Vladu, M. Reisinger, Y. Kanbur, R. Ahmed, P. Stadler, S. Bauer, N. S. Sariciftci, *Synth. Met.* **2011**, *161*, 2058.

[38] Y. Kanbur, M. Irimia-Vladu, E. D. Glowacki, M. Baumgartner, G. Schwabegger, L. N. Leonat, M. Ullah, H. Sitter, R. Schwödiauer, Z. Kücükyavuz, S. Bauer, N. S. Sariciftci, *Org. Electron.* **2012**, *13*, 919.

[39] A. l. Vasincu, E. Crețu, I. Geangalău, R. L. Mihăilescu Amalinei, A. Miron, *Rev. Med.-Chir. Soc. Med. Nat. Iasi* **2013**, *117*, 545.

[40] E. Tavčar Benković, D. Žigon, V. Mihailović, T. Petelinc, P. Jamnik, S. Kreft, *J. Wood Chem. Technol.* **2017**, *37*, 467.

[41] E. Tavčar Benković, T. Grohar, D. Žigon, U. Švajger, D. Janeš, S. Kreft, B. Štrukelj, *Ind. Crops Prod.* **2014**, *52*, 23.

[42] A. Farjon, Abies lasiocarpa, Subalpine Fir, The IUCN Red List of Threatened Species, **2013**, https://doi.org/10.2305/IUCN.UK.2013-1.RLTS.T42289A2970039.en.

[43] E. P. Favvas, E. P. Kouvelos, S. K. Papageorgiou, C. G. Tsanaktsidis, A. C. Mitropoulos, *Appl. Phys. A* **2015**, *119*, 735.

[44] W. Nong, X. Chen, J. Liang, L. Wang, Z. Tong, K. Huang, R. Wu, Q. Xie, Y. Jia, K. Li, *Adv. Mater. Res.* **2014**, *887-888*, 551.

[45] V. Beltran, N. Salvado, S. Buti, T. Pradell, *Anal. Bioanal. Chem.* **2016**, *408*, 4073.

[46] "*Impedance Spectroscopy: Theory, Experiment, and Applications*, 2nd Edition" (Eds: E. Barsoukov, J. R. Macdonald), John Wiley and Sons, Hoboken, New Jersey **2005**, https://doi.org/10.1002/0471716243.

[47] M. Egginger, M. Irimia-Vladu, R. Schwödiauer, A. Tanda, I. Frischauf, S. Bauer, N. S. Sariciftci, *Adv. Mater.* **2008**, *20*, 1018.

[48] A. H. Alami, K. Aokal, D. Zhang, A. Taieb, M. Faraj, A. Alhammadi, J. M. Ashraf, B. Soudan, J. El Hajjar, *Int. J. Energy Res.* **2019**, *43*, 5824.

[49] M. Irimia-Vladu, J. W. Fergus, *Synth. Met.* **2006**, *156*, 1396.

[50] M. Irimia-Vladu, N. Marjanovic, M. Bodea, G. Hernandez-Sosa, A. Montaigne Ramil, R. Schwödiauer, S. Bauer, N. S. Sariciftci, F. Nüesch, *Org. Electron.* **2009**, *10*, 408.

[51] A. Modafe, N. Ghalichechian, B. Kleber, R. Ghodssi, *IEEE Trans. Device Mater. Reliab.* **2004**, *4*, 495.

[52] M. Paeck, M. Woehrmann, M. Teopper, K. D. Lang, in 2019 *IEEE 69th Electronic Components and Technology Conf. (ECTC)*, IEEE, Las Vegas, NV, USA **2019**, https://doi.org/10.1109/ECTC.2019.00285.

[53] C. R. Newman, C. D. Frisbie, D. A. da Silva Filho, J. L. Bredas, P. C. Ewbank, K. R. Mann, *Chem. Mater.* **2004**, *16*, 4436.

[54] M. Zirkl, A. Haase, A. Fian, H. Schön, C. Sommer, G. Jakopic, G. Leising, B. Stadlober, I. Graz, N. Gaar, R. Schwödiauer, S. Bauer-Gogonea, S. Bauer, *Adv. Mater.* **2007**, *19*, 2241.

[55] M. Irimia-Vladu, Y. Kanbur, F. Camaioni, C. Yumusak, A. A. Vlad, C. V. Irimia, A. Operamolla, G. Farinola, G. Romanazzi, G. P. Suranna, N. González, M. C. Molina, L. F. Bautista, H. Langhals, E. D. Glowacki, N. S. Sariciftci, *Chem. Mater.* **2019**, *31*, 6315.

[56] S. Bisoyi, U. Zschieschang, M. J. Kang, K. Takimiya, H. Klauk, S. P. Tiwari, *Org. Electron.* **2014**, *15*, 3173.

[57] S. Park, E. N. Cho, I. Yun, *Microelectron. Reliab.* **2012**, *52*, 2215.

[58] U. Zschieschang, R. T. Weitz, K. Kern, H. Klauk, *Appl. Phys. A: Mater. Sci. Process.* **2009**, *95*, 139.

[59] J. Kim, J. Jang, K. Kim, H. Kim, S. H. Kim, C. E. Park, *Adv. Mater.* **2014**, *26*, 7241.

[60] M. Irimia-Vladu, E. D. Głowacki, G. Schwabegger, L. Leonat, H. Z. Akpinar, H. Sitter, S. Bauer, N. S. Sariciftci, *Green Chem.* **2013**, *15*, 1473.